Present-day bottom-current dynamics associated to the Le Danois Bank region (southern Bay of Biscay, NE Atlantic): a model in a topographically constrained small basin

Shan Liu[a*], David Van Rooij[a], Thomas Vandorpe[a, b], César González-Pola[c], Gemma Ercilla[d], Francisco Javier Hernández-Molina[e],

[a] *Department of Geology, Ghent University, Campus Sterre (building S8), Krijgslaan 281, B-9000 Gent, Belgium*

[b] *Flanders Marine Institute (VLIZ), InnovOcean site, Wandelaarkaai 7, 8400 Oostende, Belgium*

[c] *Instituto Español de Oceanografía, C.O. Gijón, Avda Príncipe de Asturias 70 bis, E-33212 Gijón, Spain*

[d] *Institut de Ciències del Mar, CSIC. Continental Margins Group-GMC. Passeig Marítim de la Barceloneta 37-49, 08003, Barcelona, Spain*

[e] *Department of Earth Sciences, Royal Holloway University, London, Egham, Surrey TW20 0EX, UK*

* corresponding author.

Tel: + 32 9 264 4591.

E-mail address: Shan.Liu@Ugent.Be (S.Liu).

Present address: Department of Geology, Ghent University, Campus Sterre (building S8), Krijgslaan 281, B-9000 Gent, Belgium.

Abstract

The present-day morphology of the Le Danois Bank region has been investigated based on bathymetric and high to ultra-high resolution seismic reflection data. The involved bottom-current processes are associated with the Eastern North Atlantic Central Water, the Atlantic Mediterranean Water and the Labrador Sea Water. Sediments originating from various canyon systems along the Cantabrian Margin and the Asturias continental shelf are transported by downslope and alongslope processes towards the Le Danois intraslope basin. The background flow velocities of bottom currents are all below the threshold of generating contourite features. However, bottom currents are locally accelerated due to the presence of the Le Danois Bank and the Vizco High, creating six plastered drifts, three elongated mounded and separated drifts, a furrow and three moats at different depth intervals. The extension and distribution of the drifts are controlled by slope morphology and/or bottom current velocities. Unlike other contourite drifts along continental slopes, a single contourite drift (the Gijón Drift) with a lateral variation in drift geometry and internal structure indicates the interaction of bottom currents with different dynamics. Additionally, scouring of active bottom currents and rapid sedimentation rate of contourite drifts are linked to slope instability events. Besides contourite drifts, internal waves induce the formation of sediment waves. In the Le Danois intraslope basin, multiple sedimentary processes work together and shape the present-day seafloor. Bottom currents are focused due to deflection on topographical features and create a wide variety of sedimentary features, including contourite drifts. These have more frequent lateral variations, a feature typical for topographically constrained small basins.

Keywords: bottom currents, contourites, southern Bay of Biscay, small basin.

1 Introduction

Bottom currents, being currents flowing near the bottom of the ocean (Faugères and Stow, 1993) can be classified based on their driving forces. Examples are thermohaline circulation, wind-driven currents, geostrophic currents, etc. (Rebesco et al., 2008). Bottom currents generated by thermohaline circulation are described as semi-permanent alongslope currents (Rebesco et al., 2014). Alongslope bottom currents are capable of suspending, transporting and/or controlling the deposition of sediments at the seafloor (Stow et al., 2002). Sediments deposited or significantly affected by bottom currents are known as contourites, and the sedimentary bodies they create are called contourite drifts (Faugères and Stow, 1993; Faugères et al., 1999; Stow et al., 2002). Bottom currents are also capable of creating erosional/non-depositional features such as contourite channels and moats (Rebesco et al., 2014; Hernández-Molina et al., 2016). The lateral and temporal variations of these contourite deposits (drifts) associated with a variety of erosional features lead to the definition of the Contourite Depositional System (CDS) (Hernández-Molina et al., 2008).

During the last two decades, numerous studies have focused their attention on large margin-scale contourite deposits, such as the well-studied Cádiz CDS along the SW Iberian continental margin (Llave et al., 2001, 2006; Stow et al., 2013), the Lofoten and Vesterålen Drifts along the NW European Atlantic margin (Laberg et al., 2005; Stoker et al., 2005) and the giant CDS along the Argentine continental margin (Preu et al., 2012, 2013). Bottom-current processes associated to these large-scale drift systems, generated by the interaction of large thermohaline currents or geostrophic currents are being widely investigated (Maldonado et al., 2005; Hernández-Molina et al., 2010). However, small-scale bottom-current intensifications in smaller basins and around topographical obstacles received far less attention and their mechanisms are not yet fully understood (Turnewitsch et al., 2004; Rebesco et al., 2014; Van Rooij et al., 2016; Zhang et al., 2016).

Small-scale contourite drifts have mostly been documented in the NE Atlantic Ocean up to now. They are reported around the mud volcanoes of the Moroccan Atlantic margin (Vandorpe et al., 2016) and the Gulf of Cádiz (Palomino et al., 2016), around the Pontevedra obstacle in the Galicia Bank region (Ercilla et al., 2011; Zhang et al., 2016), associated to cold-water coral mounds in the Porcupine Seabight, SW of Ireland (Van Rooij et al., 2007) and associated to the Le Danois Bank along the northern Iberian

continental margin (Van Rooij et al., 2010). Whereas the steep northern flank of the Le Danois Bank is dominated by gravitational processes, the intraslope basin hosts small-scale contourite deposits. The related drift systems extend from the Le Danois Bank (in the north) to the Asturias continental upper slope (in the south) and are dominating the geomorphology of the present intraslope basin. Based on some sparsely distributed seismic profiles, these drift systems seem to be highly affected by the interaction between the intermediate water mass and the associated morphologies of the intraslope basin (Ercilla et al., 2008; Iglesias, 2009; Van Rooij et al., 2010). Types and dimensions of depositional, erosional and mixed features show remarkable variations: elongated mounded and separated drifts (the Le Danois and the Gijón Drifts), plastered drifts, moats (the Le Danois and the Gijón Moats) and slide scars have all been identified (Iglesias, 2009; Van Rooij et al., 2010). However, the dynamic interaction between the present-day bottom-current circulation and the detailed characteristics, as well as the spatial variability of the drift systems are still not fully understood.

Due to the presence of a topographic obstacle (e.g. a coral bank, slide scar or fault), bottom currents will enhance locally and have the capability of creating flow filaments, in turn creating their own erosional and depositional features (Stow et al., 2002, 2008; Rebesco et al., 2008, 2014). The Le Danois Bank region is ideal for investigating the relationship between various topographic obstacles, bottom current dynamics, and different contourite features. Mediterranean Outflow Water (MOW) is considered to be the most important water mass (Ercilla et al., 2008, 2011; Van Rooij et al., 2010), referring to the pure thermohaline outflow in the Gulf of Cádiz (Hernández-Molina et al., 2014). This water mass will now be referred to as the Atlantic Mediterranean Water (AMW), due to its different physical properties and dynamics (Rogerson et al., 2012; Flecker et al., 2015). The location of the Le Danois Bank region is thus key for better understanding the local interaction of the AMW with the continental slope sedimentary processes.

This study aims to provide a comprehensive description of the distribution and current morphology of various depositional and erosional features of the Le Danois Bank region. By combining previous observations with additional ones derived from more recent seismic datasets and improved insights regarding the present-day oceanographic setting, this study aims to improve the understanding of the recent interaction between topographic obstacles and bottom currents. It is postulated that contourite features of the Le Danois Bank region can provide new insights regarding the significant role of small-scale bottom-current action in shaping or controlling the seafloor morphology. As such, this study

introduces a unique model related to the responsible bottom-current dynamics in a topographically constrained small basin.

2 Regional setting

2.1 Geology and morphology

The Le Danois Bank, an E-W narrow topographic high, is located at the Cantabrian continental slope, in the southern Bay of Biscay (Fig. 1). The northern flank (mean values between 18° and 20°, reaching 34° locally) of the Le Danois Bank steeply drops into the Biscay abyssal plain, whereas the southern flank (slope gradient varying from 0.8° and 11°) is connected to the upper continental slope (Fig. 2). The presence of the Le Danois Bank creates an intraslope basin (about 65 km long and 15-25 km wide) between the bank and the Asturias continental shelf. This basin is bounded to the west by the Vizco High and to the southeast by the Lastres Canyon (Fig. 1b). The basin becomes shallower from the centre (1070 m) towards the bank (855 m) and the continental shelf (443 m).

The Cantabrian margin was deformed by compression during the Early Paleocene to the Eocene when the northward displacement of the African plate led to the Iberian-European collision, resulting in the Cantabrian-Pyrenean chain along the northern border of the Iberian plate (Boillot et al., 1979; Alvarez-Marrón et al., 1996). In the Early Oligocene, the subduction of the Iberian plate beneath the European plate, as well as shortening of the northern Iberia plate, resulted in regional extension and compression in the Bay of Biscay (Fernández-Lozano et al., 2011). The mantle exhumation and crustal thinning beneath the Cantabrian continental margin induced the formation of the Le Danois Bank and the intraslope basin (Vissers and Meijer, 2012; Cadenas and Fernandez-Viejo, 2016). At the end of the Oligocene, the collision of the Iberian and European plates halted and there is no evidence of large-scale tectonic activity in the Le Danois Bank region from the Miocene onwards (Muñoz, 2002; Vergés et al., 2002; Roca et al., 2011; Tugend et al., 2014; Cadenas and Fernandez-Viejo, 2016).

Unlike other basins in the Cantabrian continental margin, the sedimentary infill within the intraslope basin is thin and its maximum thickness is estimated at about 10 km (Boillot et al., 1979; Cadenas and Fernandez-Viejo, 2016). The Permo-Triassic sediments are mainly alluvial deposits with an important presence of evaporates (Cadenas and Fernandez-Viejo, 2016). A regional transgression during the Lower

and Middle Jurassic in the Bay of Biscay produced bituminous clays and carbonate deposits (Riaza, 1996). With the onset of seafloor spreading during the Cretaceous, a carbonate platform, containing limestones, was created (Boillot et al., 1979; Boillot and Malod, 1988; Riaza, 1996). The Eocene and Oligocene sediments originate from shallow marine settings, but an important presence of neritic limestones and calcareous sandstones has been observed (Cadenas and Fernandez-Viejo, 2016). In the Miocene units, slumps and mass-wasting deposits have been recognized, suggesting downslope processes (Ercilla et al., 2008; Cadenas and Fernandez-Viejo, 2016). The observation of contourite deposits (drifts) in the Pliocene unit suggests a shift from downslope to alongslope processes (Van Rooij et al., 2010). Confined contourite drifts have been identified in the Upper Pliocene unit and the elongated mounded and separated drifts are generated in the Middle Pleistocene unit (Van Rooij et al., 2010). The sediment supply consists of fine-grained material eroded from the Cantabrian Mountain range (Gaudin et al., 2006; Ercilla et al., 2008). Gómez-Ballesteros et al. (2014) suggested that the sediments are transported into the ocean through the Narcea and Nalón rivers (Fig. 1a) and move along the Cantabrian continental slope eastwards by means of alongslope currents.

2.2 Oceanography

Below the surface mixed layer, the present-day oceanography of the Le Danois Bank region comprises three distinct water masses; (1) The Eastern North Atlantic Central Water (ENACW) between 350 and 600 m water depth (McCartney and Mauritzen, 2001), (2) the Atlantic Mediterranean Water (AMW) between 750 and 1550 m water depth (Iorga and Lozier, 1999a, b), and (3) the Labrador Sea Water (LSW) between 1750 and 2000 m water depth (van Aken, 2000a). Between these water masses, two interfaces are located respectively at 600 to 750 m and 1550 to 1750 m water depth (van Aken, 2000a, b) (Fig. 3).

The ENACW originates at the northeast of the Azores (Pollard et al., 1996). Its subpolar branch penetrates southwards into the Bay of Biscay following an anticyclonic circulation (Pingree, 1993; Pollard et al., 1996; McCartney and Mauritzen, 2001). Its subtropical branch constitutes an eastward slope current along the northern Iberian continental slope and flows polewards (Pingree and Le Cann, 1990; van Aken, 2000b). The ENACW contains relatively small variations in temperature and salinity in the Bay of Biscay, ranging respectively between 11.8° to 12.2 °C and 35.53 to 35.58 (Haynes and Barton, 1990; Ríos et al., 1992; Pingree, 1993). The mean velocity is around 1 cm/s in the southern Bay of Biscay (Frouin et al.,

1990; Lavín et al., 2006). In the Le Danois Bank region, the ENACW has a higher velocity (10-30 cm/s) and flows eastwards along the Asturias continental upper slope (Lavín et al., 2006; González-Pola et al., 2012). Along the rim of the eastern summit of the Le Danois Bank, an anticyclonic circulation with a velocity of about 15 cm/s has been observed at the ENACW level (González-Pola et al., 2012) (Fig. 1b). This circulation cell is most likely induced by a steady background flow impinging on the topographical barrier or interaction between periodically enhanced currents and the Le Danois Bank (González-Pola et al., 2012). Its core is located at 400 m water depth with a minimum salinity of 35.5 (Fig. 3).

At a depth of about 1000 m, a core of eastward-flowing AMW is observed hugging the northern Iberian continental slope with a mean velocity of 1-5 cm/s (Iorga and Lozier, 1999a). In the Le Danois Bank region, its maximum salinity reaches 35.8 while the temperature remains about 10°C (Fig. 3b). Most of the AMW flow penetrates along the northern flank of the Le Danois Bank and there is no dominant flow within the intraslope basin at present day (González-Pola, personal communication). The intraslope basin has the capability to develop its own recirculation pattern, due to the topographic constraints of the Le Danois Bank and the continental shelf (González-Pola et al., 2012). Anticyclonic recirculation during upwelling conditions and cyclonic recirculation during downwelling conditions have been observed at the AMW level between the bank and the continental shelf (González-Pola, personal communication) (Fig. 1b). At the eastern edge of the Le Danois Bank, a pronounced anticyclonic circulation, potentially caused by eddy shedding from the shelf, is also observed at the AMW level (González-Pola et al., 2012) (Fig. 1b). It symmetrically distributes over the bank and has a mean velocity of 10 cm/s (González-Pola et al., 2012).

Below the AMW, the LSW penetrates along the northern Iberian continental margin from east to west (Lazier, 1973; Gascard and Clarke, 1983; van Aken, 2000a). In the study area, the core of the LSW is recognized at 1800 m water depth with a minimum salinity of 35.05 (Figs. 3b, f). Due to the depth of the intraslope basin (max. 1720 m), the LSW is hindered and fails to penetrate the basin towards the west. Intense diapycnal mixing, resulting from the highly energetic internal tidal waves, has been observed between the LSW and the AMW over the Cantabrian continental slope (Pingree, 1993; van Aken, 2000a, b). This mixing action makes the Le Danois Bank region a focal point for the occurrence of the high-energetic turbulent events at the interface between the AMW and the LSW (van Aken, 2000b; Lavín et al., 2006).

3 Material and methods

Three sets of reflection seismic data have been used for this study (Fig. 1b). These datasets embrace different vertical resolutions, ranging from high to ultra-high. These different datasets contain nearly overlapping NNE-SSW to N-S orientated profiles, enabling a more detailed seismic interpretation of the morphological features. The ultra-high resolution TOPAS (topographic parametric sonar) profiles were obtained with the PS 018 system during the BIO Hespérides campaign MARCONI II in 2003 (Ercilla et al., 2008; Iglesias, 2009). The TOPAS PS 018 system is a hull-mounted seabed and sub-bottom echosounder based on an EM 122 receiver array. The penetration of the acoustic signal varies between 0 and 200 ms two-way travel time (TWT) at full oceanic depth. The primary frequency was 15 kHz (secondary 0.5-6 kHz), while the maximum vertical resolution was about 0.2 m. Four S-N trending and three E-W trending TOPAS lines were acquired in the study area with a mean spacing of 25 km. The high-resolution single-channel sparker seismic profiles were obtained during the R/V Belgica cruise ST1118a in June 2011. A 500 J energy SIG sparker (120 electrodes) has been used, with a shot interval of 2.5 s. The penetration depth of the acoustic signal varies around 500 ms TWT. The dominant frequency was around 800 Hz. The sampling frequency was set at 10 kHz and a record length of 2.2 s TWT was used. The standard vertical resolution varies around 1.5 m. Twelve NNE-SSW and fifteen W-E to WNW-ESE orientated sparker seismic lines with a spacing of 3-5 km have been acquired. The three-channel airgun seismic records have been acquired during the MARCONI II campaign. The seismic source, a 5-meter-long airgun array of 6 Sercel G-GUN II (140 bars), was located at 2.5 m depth with a shot interval of 6 s. The receiver system was a 150 m SIG streamer with 3 sections of 40 hydrophones each. The penetration of the acoustic signal is about 1.5 s TWT. The dominant frequency was around 80 Hz. The sampling frequency was 5 kHz and the recording length was 4.5 s TWT. The standard vertical resolution was about 4.5 m. Seventeen NNE-SSW and nine WNW-ESE orientated airgun seismic lines with a spacing of 10-15 km were surveyed.

The TOPAS and sparker seismic data have been processed using the DECO Geophysical RadexPro Software. A spherical divergence correction and an amplitude correction of 3 dB/ms were applied in order to compensate for the loss of energy of the seismic wavelet. A burst noise removal has been applied to remove electrical noise as well. The sparker seismic data was further processed using a static correction (swell filter) and an Ormsby bandpass filter with a low-cut ramp of 160 to 250 Hz and a high cut ramp of 1400 to 1500 Hz. The airgun seismic data was preliminarily processed on board using the Delph Seismic

Plus Software and included a bandpass filter (2.5 kHz high pass and 80 kHz low pass). Afterwards, the data were processed by applying a spherical divergence correction, an interactive velocity analysis, and a burst noise removal.

The multibeam data had been acquired with the RV Vizconde de Eza in 2003 within the framework of the ECOMARG project (http://www.ecomarg.com/). The positioning data was provided by Seapath 204, while the SIMRAD EM 300 provided the bathymetric data. This system operated at a water depth ranging between 200 and 3000 m and had a vertical error of less than 1 %. The sampling frequency was set at 30 kHz. Calibration and correction have been applied using SIMRAD NEPTUNE package and CARAIBES software. The footprint is 15 x 15 m at 500-600 m and 25 x 25 m at about 1000 m. The data covered an area of 5530 km^2. It encompasses the entire study area including the Le Danois Bank, the intraslope basin, the Vizco High, the Lastres Canyon and the adjacent continental shelf (Fig. 2).

4 Results

In the Le Danois Bank region, the most pronounced physiographic features were already reported by Ercilla et al. (2008) and Van Rooij et al. (2010). Based on these previous results, the combination of three currently available seismic datasets, the multibeam data and the updated classification of contourite drifts presented in Rebesco et al. (2014), new insights have been provided on morphosedimentary characteristics of alongslope, downslope and mixed features and their distribution.

4.1 Alongslope features

4.1.1 Elongated mounded and separated drifts

The SW-NE oriented Le Danois Drift is located between 790 and 1080 m water depth (Figs. 4, 5a, b, c). The drift encompasses an area of 242 km^2 and is about 42 km long and 4-11 km wide and 50 m high. The main element characterizing this drift is the high mounded geometry (slope gradient of 0.5° to 2.8°) (Fig. 2). Internally, it comprises continuous parallel-stratified reflections, onlapping upslope with a sigmoidal-oblique progradational pattern towards the Le Danois Bank (Fig. 5c). Towards the south, the mean thickness laterally decreases from 280 to 130 ms TWT. At the western limit of the Le Danois Drift, the thickness reaches its minimum (10-20 ms TWT).

The NW-SE oriented Gijón Drift is located at the southernmost part of the intraslope basin between 320 m and 1060 m water depth (Figs. 4, 5a, b, d). The drift is 34 km long and 2 to 13 km wide. It displays a broad mounded geometry (slope gradient of 1° to 3°) and a basal unconformity with onlap terminations (Fig. 5d). The mounded part rises 80 m above the surrounding seafloor. The seismic facies of the Gijón Drift is characterized by stratified layers of continuous sigmoidal reflections interbedded with discontinuous low-amplitude chaotic reflections (Figs. 5a, d). Towards the north, the sedimentary bodies of the Gijón and the Le Danois Drifts overlapped, where the seismic reflections are continuous parallel-even configurations (Fig. 5a). The thickness of the Gijón Drift gradually decreases from 320 to 30 ms TWT towards the southeast. The southeast extension of the Gijón Drift is limited by the presence of the Lastres Canyon (Fig. 4). Towards the northwest, the geometry of the Gijón Drift evolves from elongated and mounded (Figs. 5a, d) to confined and mounded (Fig. 5b). The change of the geometry is associated with a reduction in thickness (from 220 to 110 ms TWT). The internal structure of this part of the Gijón Drift is characterized by convex-upward seismic patterns with high- to medium-amplitude sigmoidal reflections thinning towards the edges (Fig. 5b).

At the centre of the intraslope basin, a small elongated mounded and separated drift is identified (Fig. 5c). Based on the proximal physiographic feature, the Asturias continental shelf, it is referred to as the Asturias Drift (Fig. 4). The Asturias Drift covers an area of 21 km^2 at water depths between 900 and 1080 m. It is characterized by an unconformity surface with onlap and downlap terminations and mounded geometry (slope gradient of about 1°) (Figs. 2, 5c). The drift displays a sigmoidal-oblique seismic stacking pattern (Fig. 5c). The maximum thickness is 90 ms TWT, decreasing towards the southwest.

4.1.2 Plastered drifts

Along the upper continental slope, WNW-ESE trending plastered drift 1 is identified between 200 and 500 m. It encompasses an area of about 48 km^2 and has a length of about 7.5 km and a width of 1.5-2.5 km (Figs. 2, 4, 5d). The drifts are characterized by sigmoidal reflections draped over the upper continental slope and is about 10 to 90 ms TWT thick. At the southern flank of the Le Danois Bank, four E-W trending narrow plastered drifts are recognized at different water depths. Plastered drifts 2 (9 km long and 2.4 km wide, from 528 to 642 m) and 3 (9.3 km long and 0.8 km wide, from 715 to 782 m) are located at the western edge of the Le Danois Bank and are separated by a ridge (Figs. 4, 6a). The ridge (10 km long, 600

m wide) rises 20 m above the surrounding seafloor with a WNW-ESE orientation. Plastered drift 4 (from 870 to 1100 m) is positioned at the upper southeast flank of the bank and has a length of 10 km and a width of 0.8 to 1.1 km (Figs. 2, 6b, c). Plastered drift 5 (from 1350 to 1780 m), located at the lower southeast flank of the bank, is 7 km long and 1.8-3.9 km wide (Figs. 2, 4, 6d). Along the southeast foot of the Le Danois Bank, the SW-NE oriented plastered drift 6 is located at water depths between 1760 and 1920 m (Figs. 2, 4, 6e). This plastered drift covers an area of 56 km^2 and is about 18 km long and 1.8 km wide. The thickness ranges from 20 to 60 ms TWT. The internal structure is characterized by sigmoid reflection configurations and an unconformity surface with onlap and downlap terminations.

4.1.3 Moats and furrows

The Le Danois Moat parallels the southern foot of the Le Danois Bank between 866 and 1530 m water depth (Figs. 5a, b, c). It separates the Le Danois Drift from the bank along a WNW-ESE linear trend (Fig. 4). The Le Danois Moat is about 42 km long. It has a U-shaped profile with widths ranging from 1.9 to 2.2 km and depths from 20 to 80 m (Figs. 5a, c). Towards the west, the moat narrows to a minimum width of 400 m.

The NW-SE oriented Gijón Moat separates the Gijón Drift from the upper continental slope (Fig. 4). This moat (from 320 to 1090 m) starts at the southern foot of the Vizco High and extends towards the Lastres Canyon. It deflects to the southeast and loses expression to the east. The northwest part of the moat shows an asymmetric U-shape profile (Figs. 5a, b, d) and has a depth ranging from 25 to 110 m, a width of about 2.3 km. Towards the southeast, the moat narrows to a minimum width of 800 m and the depth reduces to 10 to 20 m.

The Asturias Moat is associated with the Asturias Drift (Fig. 4). It is oriented in a W-E direction in the western part and becomes NNW-SSE towards its NE limit. The moat is about 6 km long, 400 m wide, 80 m deep and displays a V-shape profile (Fig. 5c).

A NW-SE oriented furrow occurs at the southwest edge of the Gijón Drift (Fig. 4). It can be identified on the multibeam bathymetry (Fig. 3a) and seismic reflection profiles (Fig. 5b) by its vertical incision, ranging from 10 to 20 m. The length is 4.1 km and the width is 0.8 km. It gradually loses its expression towards the southeast, as well as towards the Vizco High.

288 4.2 Downslope features

289 4.2.1 Slide scars

290 Four isolated small slide scars are identified along the southern flank of the Le Danois Bank (Fig. 4).
291 They possess relatively steep slopes (values between 6° and 18°) compared to the surrounding seafloor
292 (values between 1° and 4°) (Fig. 2). They are characterized by crescent shapes, lengths varying between
293 1.3 and 3.2 km, depths ranging between 20 and 80 m and south-dipping orientations. All of the slide scars
294 are present between 544 and 1020 m water depth (Fig. 2). The slide scars located at plastered drift 4
295 (from 840 to 877 m, slope gradient of 12°) and central part of the southern flank of the bank (from 803 to
296 854 m, slope gradient of 15°) are namely documented by Figures 6c and 7a.

297 Along the southern rim of the top of the Le Danois Bank, one large isolated slide scar with a steep slope
298 gradient of 15° to 20° has been identified (Figs. 2, 4, 6b, 7a). The headwall, between 565 and 681 m, is
299 characterized by a linear geometry (Fig. 4). This W-E orientated slide scar is about 33 km long and has a
300 mean depth of 90 m.

301 Along the southern flank of the Le Danois Moat, between 990 and 1120 m water depth, two slide scars
302 are identified based on their arcuate morphology (Figs. 2, 4, 6b). Compared to the entire southern flank
303 (mean slope gradient of 2.5°) of the Le Danois Moat, both slide scars are located on the steepest slopes (7°
304 to 9.5° slope). The eastern scar (2.2 km long and 60 m deep) has a north-dipping trend and an average
305 slope gradient of 8.2°. The western one (3.4 km long and 30 m deep) displays a lower slope gradient of 7.8°
306 with a northeast-dipping trend. Their associated slide deposits are characterized by onlap and downlap
307 terminations overlying an unconformity surface (Fig. 6b).

308 At the centre of the intraslope basin, a 2.7 km^2 isolated ellipse-shaped slide scar is shown on the
309 bathymetric and seismic data (Figs. 2, 4, 7b). This well-developed seafloor scarp shows a higher slope
310 gradient (3.5°) compared to the surrounding slopes (1.5°). It has a northeast-dipping trend and gradually
311 loses its expression from southwest to northeast (Figs. 2, 4). The headwall, located between 750 to 777 m
312 water depth, is about 2.5 km long and displays truncated seismic reflection configurations in the seismic
313 records. At the bottom of this slide scar, chaotic-transparent seismic reflections are present (Fig. 7b).

A series of isolated slide scars have been identified southeast of the Vizco High between 870 and 1280 m water depth (Figs. 4, 7c). They are positioned on an erosive unconformity surface and display a step-like pattern with at least 5 levels (at 1070, 1010, 960, 940 and 920 m) (Fig. 7c). These slide scars have an east-dipping trend and gradually lose their expressions from the west to the east. The seismic facies of these features are truncated reflections at their headwalls and chaotic-transparent reflections at the bottom. They have small variations in shape (arcuate), size (2.8 to 3.2 km in diameter, 20 to 60 m deep) and orientation (N-S) (Fig. 4). The slope gradient of the headwalls ranges from 7° to 13° (Fig. 2).

4.2.2 Mass-transport deposits

A large area (233 km^2) of mass-transport deposit is located between the Le Danois Drift, the Gijón Drift and the Lastres Canyon (Fig. 4). The identification is based on a distinctive seafloor irregularity and discontinuous low-amplitude chaotic and transparent reflections in the seismic records (Figs. 2, 7d). The boundary of these mass-transport deposits has a relatively sharp slope gradient (about 4.5°) compared to the surrounding area (about 0.8°) (Fig. 2).

4.3 Topographic irregularities and morphological depressions

At the northeast edge of the Gijón Moat, an ellipse-shaped morphological depression is identified between 680 and 770 m water depth (Fig. 7e). It is 5.5 km in diameter and 30 to 80 m deep with a NW-SE orientation. A pronounced scarp (about 20 m deep) occurs within this depression (Fig. 7e). The scarp is characterized by an erosive unconformity surface and truncated reflections. Undulating wavy-oblique reflections make up the succession between the seafloor and the unconformity surface in the seismic records. The wave-crest features are about 1-2 km long, 200 m wide and rise 10 m above the surrounding areas with a trend of upslope migration.

At the centre of the intraslope basin, a remarkable asymmetric ear-shaped depression is identified between 990 and 1080 m water depth (Figs. 4, 7f). It is 6 km in diameter and has a northwest-dipping trend. The upslope facing flank is 20 to 90 m deep with a slope gradient of about 18° (Fig. 2). It is characterized by truncation of parallel-stratified reflections (Fig. 7f). This depression delimits an oblique terrace (2.3° slope) with wavy morphology along the downslope facing flank. The related terrace displays

high-amplitude chaotic reflections overlain by continuous wavy-stratified reflections (Fig. 7f). These wave-like features are about 2.5-3.5 km long, 400 m wide and rise 30 m above the surrounding seafloor.

Several topographic irregularities and morphological depressions (from 1540 to 2100 m) occur between the Le Danois Drift, plastered drift 6 and the Lastres Canyon. The identification is based on their irregular shapes (circular, crescent and ellipse-shaped), sizes (0.8 to 3.7 km in diameter, 40 to 80 m deep), slope gradients (values between 15° and 22°) and orientations (WSW-ENE to NW-SW trending) (Figs. 2, 4). Only a few seismic profiles document these depressions. They are characterized by truncated, chaotic, semi-transparent or wavy-stratified reflections (Fig. 5e).

5 Discussion

5.1 Present-day bottom-current implications on contourite features

The present-day bottom-current circulation within the Le Danois intraslope basin is dominated by three water masses: the ENACW, the AMW and the LSW. Due to their different physical characteristics and circulation patterns, they may play a significant role in shaping the present-day depositional and erosional contourite features. The combination of the CTD data (World Ocean Database, 2013) and the interpreted seismic profiles (Figs. 5, 6, 7) allow gaining more insights regarding the interaction between each water mass and its impact on the local seabed (contouritic) processes.

5.1.1 ENACW processes

The ENACW (flowing between 200 and 570 meters water depth) mainly interacts with the upper continental slope and the upper southern flank of the Le Danois Bank, where plastered drifts 1 and 2, 3 are respectively located (Figs. 8a, b, c). Deposition of plastered drifts requires a velocity of 10-30 cm/s of bottom currents (Stow et al., 2002). As such, bottom currents associated with plastered drifts 1, 2 and 3 should be up to >10 cm/s. Indeed, present-day bottom currents along the southern flank of the bank in that depth interval are approximately 15 cm/s (González-Pola et al., 2012). There are no known measurements of velocities of bottom currents around plastered drift 1. However, along the Asturias continental slope, the ENACW generally has a mean velocity of 10-30 cm/s (González-Pola et al., 2012). All of these values meet the conditions set by Stow et al. (2002) for generating plastered drifts, and related

366 bottom currents are most likely resulted from the ENACW circulation documented by González-Pola et al.
367 (2012) (Fig. 9). Additionally, plastered drifts 2 and 3 are distributed along the northern and southern foot
368 of a ridge (Fig. 6a) with similar orientations, shapes and lengths. These features illustrate similar bottom-
369 current processes resulting from interactions between small flow filaments and the adjacent topographic
370 obstacle. The related bottom-current dynamics could be compared with the present-day anticyclonic
371 circulation cell along the western rim of the Le Danois Bank (González-Pola et al., 2012) (Fig. 9).

372 Slope morphology is one of the main elements responsible for the formation of plastered drifts as well
373 (Laberg and Camerlenghi, 2008). At the eastern edge of plastered drifts 2 and 3, the slope gradient
374 abruptly increases to 8.5°. This steep slope is maintained to the southeast flank of the bank (Fig. 2). Higher
375 slope gradients could accelerate bottom currents, in turn shifting sedimentary processes from deposition
376 to non-deposition/erosion (Rebesco et al., 2014). These higher slope angles could inhibit the generation of
377 plastered drifts along this part of the Le Danois Bank. Towards the eastern boundary of plastered drift 1,
378 the slope gradient maintains but the space between the lower continental slope and the Asturias
379 continental shelf is widened (Fig. 2). The wide morphology will decelerate bottom currents (Faugères and
380 Stow, 2008). Bottom currents could drop to <8 cm/s and slower flows limit the lateral extension of
381 plastered drift 1 towards the east.

382 5.1.2 AMW processes

383 The AMW mainly interacts with the southern flank of the Le Danois Bank and the intraslope basin
384 between 750 and 1500 m water depth (Fig. 8). Plastered drift 4 (from 870 to 1100 m) is positioned along
385 the upper southeast flank of the Le Danois Bank (Figs. 6b, 8d), where bottom currents are estimated at 10-
386 15 cm/s (González-Pola et al., 2012). This drift covers a gentle slope (mean slope gradient of about 3.6°)
387 (Fig. 2) and is shaped by the AMW (Fig. 9). Along the entire boundary of plastered drift 4, the slope
388 gradients abruptly increase to 8-15° (Fig. 2), delineating its extent. Considering all, slope morphology is
389 the main controlling factor for the spatial distribution of plastered drift 4.

390 The Le Danois Drift (from 790 to 1080 m) is suggested to be generated by the AMW as well. The
391 associated Le Danois moat indicates a focused flow pathway of bottom currents all along the southern foot
392 of the Le Danois Bank. This feature matches with the present-day oceanographic data documented by

González-Pola et al., (2012). A 12-month long mooring record (at 44°02.33', N 4°49.33' W) indicates a persistent westward near-bottom flow along the southern foot of the bank at the AMW level (González-Pola et al., 2012). The flow commonly exceeds 20 cm/s (González-Pola et al., 2012), which is sufficient to generate associated contourite drifts (Stow et al., 2002, 2009). Towards its western limit, the Le Danois Drift extends to an open area between the lower continental slope and the intraslope basin (Fig. 4). In this area, the Le Danois bank is absent and bottom currents most likely will drop to the reported background values, which are less than 5 cm/s (Iorga and Lozier, 1999a). Towards the eastern limit of this drift, the presence of a group of morphological depressions limits the distribution of the Le Danois Drift (Fig. 4). Consequently, slower bottom currents and seabed morphology limit the distribution of the Le Danois Drift. The Le Danois Drift and plastered drift 4 have similar orientations and are located at the same water depths (Figs. 4, 9). The distribution suggests that the associated bottom-current processes of both drifts are related to the same current (Fig. 9). The presence of two types of contourite drifts along the AMW pathway can be explained by changes in current velocities (Faugères and Stow, 2008). This implies accelerated and then decelerated processes from the southeast towards the southwest flank of the Le Danois Bank.

The Gijón Drift and the Moat extend from 320 to 1090 m water depth. A CDS is usually associated to one water mass (Rebesco et al., 2014). However, at the present day, the Gijón Drift is situated within the boundaries of two different water masses, being the ENACW and the AMW (Figs. 8a, b, c). Along the Cantabrian continental upper slope, the ENACW is impossible to sink to 1000 m for prolonged periods of time (McCartney and Mauritzen, 2001), while the AMW could only reach up to 400 m during interglacial climate cycles (Zhang et al., 2016; Kaboth et al., 2016, 2017). Additionally, shape and morphology of the Gijón Drift display different features in different depth intervals. Within the ENACW, the Gijón Drift has elongated and mounded geometry (Figs. 8b, c), whereas the part within the AMW is confined and mounded (Fig. 8a). Different shapes of contourite drifts are related to different bottom-current conditions (Faugères and Stow, 2008). As such, it is possible that the ENACW and the AMW interacted with the upper continental slope during different climate intervals and both are responsible for the Gijón Drift.

The spatial variation of the Gijón Drift could be controlled by the slope morphology as well. On the multibeam bathymetry, the Gijón Moat (NE-SW trending) does not fit the alongslope distribution compared to the Asturias continental slope (WNW-ESE trending) (Figs. 3a, 4). The obliquity may be

caused by the presence of the Gijón Canyon (NE-SW trending) (Figs. 4, 8f). Interactions between canyon channels and bottom currents are possible to provoke streamline distortions and accelerate current flows (Holland, 1972). The related distortion and acceleration enable bottom currents flowing upwards along canyon channels (Jackson et al., 2006). When the AMW encounters the Gijón Canyon, bottom currents could follow the canyon morphology (Allen and De Madron, 2009; Muench et al., 2009) and arise towards the shallower continental slope (320 m water depth). The variation of the Gijón Drift could also link with the interaction between the Gijón Canyon and the AMW.

The Asturias Drift lies around a buried structural high at the centre of the intraslope basin (Figs. 4, 5c, 8c). The presence of a topographical obstacle can create faster currents, in turn generating contourite depositional and erosional features (Ercilla et al., 2016; García et al., 2016). The associated Asturias Moat indicates the pathway of bottom currents. The W-E to NNW-SSE deflection of the moat may result from the morphological control of the associated depression (Fig. 9). As such, the Asturias Drift and Moat result from interactions of the AMW with a buried structural high and a morphological depression. Related bottom-current processes could be linked with the present-day AMW circulation cell (González-Pola et al., 2012) in the intraslope basin (Fig. 9).

At the southeast edge of a group of slide scars, a furrow is located in the Gijón Drift at water depths of 844 to 870 m (Figs. 4, 5b). Present-day bottom currents associated to the AMW in the intraslope basin (from 10 to 20 cm/s, González-Pola et al., 2012) do not have sufficient energy to create erosive furrows, which require at least 30 cm/s (Stow et al., 2009). However, it is well documented that the presence of topographic obstacles or irregularities can cause locally intensified bottom currents (Rebesco et al., 2008, 2014). Examples include the Galicia Bank region where intensifications from 7 cm/s up to 35 cm/s are recorded (Zhang et al., 2016), the Porcupine Abyssal Plain where accelerations reach 15 cm/s (Turnewitsch et al., 2004), and the Xisha Trough where enhancements from 15 cm/s up to 30 cm/s are documented (Chen et al., 2016). Similarly, bottom currents can recirculate around the Vizco High, possibly speeding up from 10-20 cm/s to over 30 cm/s in this region. The presence of the furrow indicates faster bottom currents resulted from strong interactions with the Vizco High.

448 5.1.3 LSW processes

449 The LSW is only present between the Lastres Canyon and the lower southern flank of the Le Danois
450 Bank in the study area (below 1750 m water depth) (Figs. 3f, 8). Plastered drifts 5 is located along the
451 lower southern flank (2.4° slope) while plastered drift 6 lies along the southeastern foot (1.2° slope) of the
452 bank (Figs. 2, 4, 8e). Both lay within the depth windows of the LSW. Along the Cantabrian continental
453 slope, the bottom current velocities (2-6 cm/s; Speer et al., 1999; Friocourt et al., 2007) are below the
454 threshold for depositing plastered drifts (Stow et al., 2002, 2009). Consequently, the presence of these two
455 plastered drifts indicates local intensification. Since there are no known measurements of current
456 velocities at this depth interval in the study area, bottom currents generating these plastered drifts have
457 to be estimated. The threshold for deposition of plastered drifts is 10 cm/s (Stow et al., 2009), so local
458 current velocities must exceed this value. Along the entire boundary of plastered drift 5, slope gradients
459 increase to 6°-10° (Figs. 2, 4). As such, steeper slope morphologies control and limit the distribution of
460 plastered drift 5. The extension of plastered drift 6 is limited by seafloor depressions positioned between
461 the bank and the Lastres Canyon (Fig. 4). Towards the northeast boundary of plastered drift 6, the
462 presence of a topographic high locally creates slopes from 1° to 11° (Fig. 2). These slopes limit the
463 distribution of plastered drift 6.

464 5.2 Interaction with slope instability processes

465 In the study area, plenty of slide scars occur at the surfaces of contourite drifts and along the southern
466 flank of the Le Danois Bank (Figs. 2, 4). The main causal factors for submarine slides include high slope
467 angles, seismic activity, volcanic activity, gas charging and rapid sediment accumulation (Locat and Lee,
468 2002; Sultan et al., 2004; Verdicchio and Trincardi, 2008; Miramontes et al., 2016; Rashid et al., 2017).
469 Since no seismic or volcanic activity and gassy sediments have been observed in the study area, the
470 triggering mechanisms for these slide scars are either rapid sediment accumulation or oversteeping.

471 5.2.1 Increased sediment accumulation

472 An isolated slide scar is positioned at the northeast part (3° slope) of the Gijón Drift (Figs. 2, 7b). The
473 sedimentation rate of the Gijón Drift is unknown. However, mounded drifts are known to have relatively
474 high sedimentation rates (5-60 cm/ka) compared to pelagic (<2 cm/ka) and hemipelagic (5-15 cm/ka)

475 sediments (Stow et al., 2008). During the build-up of the Gijón Drift, high sedimentation rates are capable
476 of decreasing shear resistance stresses of sediments, inducing mass-wasting events (Baeten et al., 2013).
477 Since the slide scar lies between the Asturias Drift and the Gijón Drift (Fig. 4), two drift systems can
478 deliver sediments to this location and drastically increase the sedimentation rate. As such, the occurrence
479 of a slope instability event at this location is more likely, compared to other areas of the Gijón Drift.

480 Opposed to the Gijón Drift, no slope instability processes occur at the surface of the Le Danois Drift (Figs.
481 2, 4). The difference between both drifts may be related to their internal depositional structures.
482 Interbedded continuous sigmoidal reflections and discontinuous low-amplitude chaotic reflections within
483 the Gijón Drift are interpreted as interbedded mass-transport and contourites deposits (Figs. 5a, d),
484 whereas only contourites are present within the Le Danois Drift (Figs. 5a, c). Similar examples of
485 interbedded structure within contourite drifts have been documented in the vicinity of the Storegga Slide
486 region (glacigenic/contouritic deposits), offshore Norway (Bryn et al., 2005) and in the Afen Slide area
487 (mud/sand contouritic deposits), offshore UK (Wilson et al., 2004). Based on borehole and core data from
488 these areas, different physical properties of sediments result in specific sedimentation layers with higher
489 sensitivity (Kvalstad et al., 2005; Laberg and Camerlenghi, 2008). Higher sensitive layers can effectively
490 reduce shear resistance strength of sedimentary bodies and thus a dynamic slide process can initiate
491 (Kvalstad et al., 2005). Within the Gijón Drift, interbedded mass-transport deposits and contourites create
492 high sensitive layers and induce mass movements. Conversely, the shear strength of the Le Danois Drift is
493 not low enough to trigger slope instability events.

494 5.2.2 Scouring of active bottom currents

495 Two slide scars occur at the southern flank of the Le Danois Moat (Figs. 2, 4). Both slide scars are
496 distributed along the steepest (9°) parts of the moat (Fig. 2). The focused flow within the Le Danois Moat
497 could be held responsible for the formation of these slide scars. Similar to the Cape Basin, where a slide
498 scar is induced by scouring of bottom currents (Weigelt and Uenzelmann-Neben, 2004), higher angles and
499 active bottom currents can provide favourable conditions for slope instability processes in this part of the
500 moat. The associated slide deposits display internal structures with onlap and downlap terminations and
501 their geometry resemble patched drift features (Fig. 6b), hinting towards reworking of bottom currents.
502 The observed features in the study area are similar to recent discoveries in the Guadalquivir Bank, where

503 reworking of bottom currents reshaped the slide deposits (García et al., 2016). In conclusion, focused
504 bottom currents within the Le Danois Moat locally scour the steeper flank, this lead to the loss of
505 downslope support and shear strength of the upslope sediment, triggering sliding and mass movements.
506 Between the northwest end of the Gijón Drift and the Vizco High, a series of slide scars overlay a steep
507 slope (10°) (Figs. 2, 7c). These slide scars are located below the pathway of the AMW currents (Fig. 9).
508 Scouring of active bottom currents is capable of producing steeper slopes, which makes this location
509 prone to slope instability events.

510 5.2.3 Mixed processes

511 In the Le Danois Bank region, a large area of mass-transport deposits lies between the Lastres Canyon,
512 the Gijón and the Le Danois Drifts (Fig. 4). The mass movements initiate from the Asturias continental
513 upper slope (Fig. 7d). The slope gradient (9.5°) of this location is much higher than the surrounding
514 seafloor (2.8°) (Fig. 2). High slope angles lead to downslope processes at this particular location. Towards
515 the east, the orientation of this mass-transport deposits area gradually changes from downslope (N-S
516 trending) to alongslope (W-E trending) directions (Fig. 4). This deflection indicates the interaction
517 between mass movements and AMW currents (Fig. 9). Characteristics of these mass-transport deposits
518 can be compared to those at the southeast Grand Banks (Rashid et al., 2017) and along the Mid-Norwegian
519 Margin (Bryn et al., 2005), where the area of mass-transport deposits is elongated and enlarged by bottom
520 currents. As such, these mass-transport deposits are triggered by high slope gradient and influenced by
521 bottom currents resulting from the AMW (Fig. 9).

522 5.3 A genetic model for the sediment waves of the Le Danois Bank region

523 Within the intraslope basin, wavy features are identified in the seismic records (Figs. 6e, 7e, f). These
524 features are interpreted as sediment wave fields (respectively A, B and C on Fig. 4) based on the traceable
525 and continuous seismic reflections, as opposed to slope failure deposits with sharp and acoustically
526 incoherent reflections (Gardner et al., 1999; Lee et al., 2002; Mosher and Thomson, 2002; Wynn and Stow,
527 2002). The formation of sediment waves has three possible causes, being turbidity currents, bottom
528 currents or internal waves (Ercilla et al., 2002; Ribó et al., 2016). Since the study area lacks the presence of
529 turbidite processes, these sediment wave fields most likely result from bottom currents or internal waves.

Sediment wave field A is located within the AMW level and is induced by internal waves. Bottom currents can be ruled out as the moat in the vicinity of sediment wave field A suggests N-S oriented bottom currents (Fig. 9), which is parallel to the wave crests. This orientation does not fit the bottom-current induced sediment waves (oblique or perpendicular orientations of the wave crests; Masson et al., 2002; Wynn and Masson, 2008).

Sediment waves created by internal waves are documented in several regions (Pomar et al., 2012; Delivet et al., 2016; Ribó et al., 2016). When internal waves propagate down a sloping bottom, three possible reflection conditions exist based on the propagation angle of the internal wave (c) and the bottom slope angle (γ) (Cacchione et al., 2002). The relationship was established by Cacchione and Wunsch (2006) and can be written as:

$$c = arctan\left[\left(\frac{\sigma^2 - f^2}{N^2 - \sigma^2}\right)^{\frac{1}{2}}\right]$$

where σ is the internal wave frequency, f is the local Coriolis (inertial) frequency, and N is the Brunt–Väisälä (buoyancy) frequency. Different values of γ/c correspond to subcritical ($\gamma/c < 1$), critical ($\gamma/c \approx 1$) and supercritical ($\gamma/c > 1$) reflection conditions (Lamb, 2014). In the study area, high-frequency internal waves have been observed near the centre of the intraslope basin at the level of the AMW (González-Pola et al., 2012). Based on the local flow properties, González-Pola et al. (2012) proposed the following parameters: f as 1.013 x 10^{-4} /s, σ as 0.09 cph and N as 1.5 to 2.5 x 10^{-3} s^{-1}. Thus, internal wave reflection condition in sediment wave field A (1.6° slope) is subcritical. Subcritical conditions of internal waves are generally characterized by smaller wave heights and upslope migration (Lamb, 2014; Delivet et al., 2016; Ribó et al., 2016). And this is true for sediment wave field A, which migrates upslope and their wave heights is relatively small (10 m) compared to those in the Argentine Basin (30 m) (von Lom-Keil et al., 2002), the Gulf of Valencia (50 m) (Ribó et al., 2016) and the Bahama Outer Ridge (60 m) (Flood and Giosan, 2002).

Sediment wave fields B (Fig. 8f) and C (Fig. 8g) are respectively located at the ENACW/AMW and the AMW/LSW interfaces. No mooring measurements have been performed at these interfaces and the present-day oceanographic dynamics are unknown. However, the mean salinity values at the ENACW/AMW (35.6) and the AMW/LSW interfaces (35.2) (Fig. 8) indicate mixing processes as the

ENACW has a mean salinity of 35.5, the AMW 35.8 and the LSW 35.1 (Fig. 3b). Turbulent mixing at the interface between water masses generally produces relatively high energetic currents associated with internal waves, which are capable of transporting and depositing sediments (Preu et al., 2013; Ercilla et al., 2016; Juan et al., 2016). The relatively small wave heights (7 and 10 m for wave fields B and C) and the observed upslope migration both indicate a subcritical reflection parameter (Lamb, 2014). As such, sediment wave fields B and C are most likely related to internal waves as well. Both sediment wave fields are located within morphological depressions (slopes of 8°-10°) (Figs. 2, 4) and overlie irregular unconformity surfaces (Figs. 6d, 7c), which are the prerequisites for the formation of sediment waves (Aghsaee et al., 2010).

5.4 Sediment sources

The sediments constituting the various drifts in the region are mainly transported by downslope processes to the continental slopes and caught by bottom currents from adjacent areas towards the Le Danois Bank region (Gómez-Ballesteros et al., 2014). One year long current meter data, obtained from the Avilés Canyon (west of the Le Danois area, Fig. 1a) indicates direct delivery of river-sourced (the Narcea and Nalon Rivers) material into the canyon and its adjacent continental slope (Rumín-Caparrós et al., 2013). Frequent severe storms and repeated cycles of semidiurnal tides regionally enhanced the bottom currents, assuring a permanent amount of sediment in suspension in the canyon region (Rumín-Caparrós et al., 2016). Additionally, the Narcea and Nalon Rivers are generated before the formation period (the Neogene, Gómez-Ballesteros et al., 2014) of the Avilés canyon (Fernández-Viejo et al., 2014). The suspended material is possible to be picked up by eastward moving water masses towards the Le Danois Bank since the intensification of the AMW (during the late Pliocene, Hernández-Molina et al., 2014) and the establishment of the Iberian Poleward Current (during the late Pleistocene, Mena et al., 2018). Consequently, the Narcea and Nalon Rivers could provide sediments for identified contourite deposits for prolonged periods of time (Gómez-Ballesteros et al., 2014; Rumín-Caparrós et al., 2016).

The Avilés Canyon is not the only sediment source for the contourite deposits. Current meter data reveal a long-term (12-month) persistent westward flow within the Le Danois Moat (González-Pola et al., 2012), which has an opposite direction compared to the major branch of the AMW (Fig. 9). Additionally, the LSW flows towards the intraslope basin in a westward direction as well (Fig. 9). These observations

585 suggest an additional eastern sediment source should be present. The Torrelavega Canyon is located in
586 the vicinity of the study area and fed by sediments from the Besaya River (Fig. 1a) (Caballero et al., 2014).
587 Eddies extending from the surface down to 3500 m water depth have been observed above the
588 Torrelavega canyon (Caballero et al., 2014), which remained stationary for a long time (locally up to 7
589 months) (Pingree and Le Cann, 1992; Caballero et al., 2014), creating the possibility for associated
590 energetic current patterns to erode the seafloor and suspend sediments (Shanmugam, 2013). As such,
591 suspended sediments can be transported towards the Le Danois Bank area by bottom currents associated
592 with the AMW and the LSW.

593 The Gijón and the Lastres Canyons can be possible sediment sources as well. Few studies have
594 documented these two canyon systems. Based on their locations, the Sella River is suggested to be the
595 sediment supply for both canyons (Fig. 1a). Erosive features at the canyon walls have been displayed in
596 the seismic records (Fig. 8f). Due to the consistent AMW flowing above the intraslope basin, eroded
597 sediments can contribute to the sediment accumulation of the prevailing contourite drifts. Finally, mass-
598 transport deposits are interbedded within the Gijón Drift (Figs. 5a, d) and indicate the interaction between
599 bottom currents and gravitational processes along the upper continental slope. These processes may add
600 sediments from the Asturias continental shelf to the contourite drifts.

601 **6 Conclusion**

602 The spatial variability of contourite drifts, slope morphology and small-scale bottom-current processes
603 are all tied together in this topographically constrained small basin. Bottom currents associated to the
604 ENACW, the AMW and the LSW are more focused and strongly intensified (acceleration up to 25 cm/s)
605 due to the morphological constraint of the Le Danois Bank and the Vizco High. Changes in velocities of
606 bottom currents and slope gradients result in variations in types, shapes and spatial distributions of
607 contourite drifts, especially along the current pathways of the AMW. Unlike typical elongated and
608 mounded drifts, the Gijón Drift exhibits a lateral variation (evolving from elongated to confined geometry)
609 at different depth intervals, which evidently indicate different bottom-current dynamics associated to one
610 contourite drift, suggesting specific geometries and shapes of contourite drifts in topographically
611 constrained small basins. Despite the influence of large topographic obstacles, small steep (slopes of 8°-
612 10°) morphologic irregularities interact with internal waves, generating small-scale (wave heights 7-10 m)

upslope-migrated sediment waves in the intraslope basin. Enhanced bottom-current processes interplay with internal waves and slope instability events, and determine the complex morphology of the present-day seafloor. Compared with large contourite features resulted from deep water masses, small basin-scale contourite features of the Le Danois Bank region is an exquisite example of multiple processes interacting in a topographically constrained basin at an intermediate water depth. The spatial variability of this system is more frequent than anticipated so far and can have far-reaching implications for comparable topographic and oceanographic settings all over the world.

Acknowledgements

This study was carried out within the framework of a Chinese Scholarship Council "CSC Grant" (201506410062). The authors wish to express our gratitude to the crews and scientific researchers of the MARCONI II, the ECOMARG and the R/V Belgica ST1118a campaigns. Shiptime RV Belgica was provided by BELSPO and RBINS–OD Nature. These research campaigns framed within the ECOMARG (REN2002-00916/MAR) and MARCONI (REN2001-1734 C03-01/M) projects. This study also builds upon achievements of project ESF Euromargins MOUNDFORCE, EC FP5 RTN EURODOM and EC FP6 HERMES (GOCE-CT-2005-511234-1).

References

Aghsaee, P., Boegman, L., Lamb, K.G., 2010. Breaking of shoaling internal solitary waves. J Fluid Mech 659, 289–317. https://doi.org/10.1017/S002211201000248X

Allen, S.E., Durrieu De Madron, X., 2009. A review of the role of submarine canyons in deep-ocean exchange with the shelf. Ocean Sci 5, 607–620. https://doi.org/10.5194/os-5-607-2009

Alvarez-Marrón, J., Pérez-Estaún, A., Dañobeitia, J.J., Pulgar, J.A., Martínez Catalán, J.R., Marcos, A., Bastida, F., Ayarza Arribas, P.A., Aller, J., Gallart, A., Gonzalez-Lodeiro, F., Banda, E., Comas, M.C., Córdoba, D., 1996. Seismic structure of the northern continental margin of Spain from ESCIN deep seismic profiles. Tectonophysics 264, 153–174. https://doi.org/10.1016/S0040-1951(96)00124-2

Baeten, N.J., Laberg, J.S., Forwick, M., Vorren, T.O., Vanneste, M., Forsberg, C.F., Kvalstad, T.J., Ivanov, M., 2013. Morphology and origin of smaller-scale mass movements on the continental slope off northern Norway. Geomorphology 187, 122–134. https://doi.org/10.1016/j.geomorph.2013.01.008

Boillot, G., Dupeuble, P.A., Malod, J., 1979. Subduction and tectonics on the continental margin off northern Spain. Mar Geol 32, 53–70. http://dx.doi.org/10.1016/0025-3227(79)90146-4

Boillot, G., Malod, J., 1988. The north and north-west Spanish continental margin: a review. Rev Soc Geol España 1, 295–316.

Bryn, P., Berg, K., Stoker, M.S., Haflidason, H., Solheim, A., 2005. Contourites and their relevance for mass wasting along the Mid-Norwegian Margin, in: Ormen Lange–an Integrated Study for Safe Field Development in the Storegga Submarine Area. Elsevier, Oxford, pp. 85–96. https://doi.org/10.1016/B978-0-08-044694-3.50011-1

Caballero, A., Ferrer, L., Rubio, A., Charria, G., Taylor, B.H., Grima, N., 2014. Monitoring of a quasi-stationary eddy in the Bay of Biscay by means of satellite, in situ and model results. Deep Sea Res Part II Top Stud Oceanogr 106, 23–37. https://doi.org/10.1016/j.dsr2.2013.09.029

Cacchione, D., Wunsch, C., 2006. Experimental study of internal waves over a slope. J Fluid Mech 66, 223–239. https://doi.org/10.1017/S0022112074000164

Cacchione, D.A., Pratson, L.F., Ogston, A.S., 2002. The Shaping of Continental Slopes by Internal Tides. Science (80) 296, 724–727. https://doi.org/10.1126/science.1069803

Cartes, J.E., Huguet, C., Parra, S., Sanchez, F., 2007. Trophic relationships in deep-water decapods of Le Danois bank (Cantabrian Sea, NE Atlantic): Trends related with depth and seasonal changes in food quality and availability. Deep Sea Res Part I Oceanogr Res Pap 54, 1091–1110. https://doi.org/10.1016/j.dsr.2007.04.012

Chen, H., Xie, X., Zhang, W., Shu, Y., Wang, D., Vandorpe, T., Van Rooij, D., 2016. Deep-water sedimentary systems and their relationship with bottom currents at the intersection of Xisha Trough and Northwest Sub-Basin, South China Sea. Mar Geol 378, 101–113. http://dx.doi.org/10.1016/j.margeo.2015.11.002

Delivet, S., Van Eetvelt, B., Monteys, X., Ribó, M., Van Rooij, D., 2016. Seismic geomorphological reconstructions of Plio-Pleistocene bottom current variability at Goban Spur. Mar Geol 378, 261–275. http://dx.doi.org/10.1016/j.margeo.2016.01.001

Ercilla, G., Alonso, B., Wynn, R.B., Baraza, J., 2002. Turbidity current sediment waves on irregular slopes: observations from the Orinoco sediment–wave field. Mar Geol 192, 171–187. http://dx.doi.org/10.1016/S0025-3227(02)00554-6

Ercilla, G., Casas, D., Estrada, F., Vázquez, J.T., Iglesias, J., García, M., Gómez, M., Acosta, J., Gallart, J., Maestro-González, A., 2008. Morphosedimentary features and recent depositional architectural model of the Cantabrian continental margin. Mar Geol 247, 61–83. http://dx.doi.org/10.1016/j.margeo.2007.08.007

Ercilla, G., Casas, D., Vázquez, J.T., Iglesias, J., Somoza, L., Juan, C., Medialdea, T., León, R., Estrada, F., García-Gil, S., Farran, M. l., Bohoyo, F., García, M., Maestro, A., 2011. Imaging the recent sediment dynamics of the Galicia Bank region (Atlantic, NW Iberian Peninsula). Mar Geophys Res 32, 99–126. https://doi.org/10.1007/s11001-011-9129-x

Ercilla, G., Juan, C., Hernández-Molina, F.J., Bruno, M., Estrada, F., Alonso, B., Casas, D., Farran, M. lí, Llave, E., García, M., Vázquez, J.T., D'Acremont, E., Gorini, C., Palomino, D., Valencia, J., El Moumni, B., Ammar, A., 2016. Significance of bottom currents in deep-sea morphodynamics: An example from the Alboran Sea. Mar Geol 378, 157–170. http://dx.doi.org/10.1016/j.margeo.2015.09.007

Faugères, J.C., Stow, D.A. V, 1993. Bottom-current-controlled sedimentation: a synthesis of the contourite problem. Sediment Geol 82, 287–297. http://dx.doi.org/10.1016/0037-0738(93)90127-Q

Faugères, J.C., Stow, D.A. V, Imbert, P., Viana, A., 1999. Seismic features diagnostic of contourite drifts. Mar Geol 162, 1–38. http://dx.doi.org/10.1016/S0025-3227(99)00068-7

Faugères, J.C., Stow, D.A. V, 2008. Chapter 14 Contourite Drifts: Nature, Evolution and Controls, in: Rebesco, M., Camerlenghi, A. (Eds.), Developments in Sedimentology. Elsevier, pp. 257–288. http://dx.doi.org/10.1016/S0070-4571(08)10014-0

Fernández-Lozano, J., Sokoutis, D., Willingshofer, E., Cloetingh, S., De Vicente, G., 2011. Cenozoic deformation of Iberia: A model for intraplate mountain building and basin development based on analogue modeling. Tectonics 30, TC1001. https://doi.org/10.1029/2010TC002719

Flecker, R., Krijgsman, W., Capella, W., de Castro Martíns, C., Dmitrieva, E., Mayser, J.P., Marzocchi, A., Modestou, S., Ochoa, D., Simon, D., Tulbure, M., van den Berg, B., van der Schee, M., de Lange, G., Ellam, R., Govers, R., Gutjahr, M., Hilgen, F., Kouwenhoven, T., Lofi, J., Meijer, P., Sierro, F.J., Bachiri, N., Barhoun, N., Alami, A.C., Chacon, B., Flores, J.A., Gregory, J., Howard, J., Lunt, D., Ochoa, M., Pancost, R., Vincent, S., Yousfi, M.Z., 2015. Evolution of the Late Miocene Mediterranean–Atlantic gateways and their impact on regional and global environmental change. Earth-Science Rev 150, 365–392. https://doi.org/10.1016/j.earscirev.2015.08.007

Flood, R.D., Giosan, L., 2002. Migration history of a fine-grained abyssal sediment wave on the Bahama Outer Ridge. Mar Geol 192, 259–273. http://dx.doi.org/10.1016/S0025-3227(02)00558-3

Friocourt, Y., Levier, B., Speich, S., Blanke, B., Drijfhout, S.S., 2007. A regional numerical ocean model of the circulation in the Bay of Biscay. J Geophys Res Ocean 112, C09008. https://doi.org/10.1029/2006JC003935

Frouin, R., Fiúza, A.F.G., Ambar, I., Boyd, T.J., 1990. Observations of a poleward surface current off the coasts of Portugal and Spain during winter. J Geophys Res Ocean 95, 679–691. https://doi.org/doi:10.1029/JC095iC01p00679

Gabriela, F.-V., Carlos, L.-F., José, D.-C.M., Patricia, C., 2014. How much confidence can be conferred on tectonic maps of continental shelves? The Cantabrian-Fault case. Sci Rep 4, 3661. https://doi.org/10.1038/srep03661

García, M., Hernández-Molina, F.J., Alonso, B., Vázquez, J.T., Ercilla, G., Llave, E., Casas, D., 2016. Erosive sub-circular depressions on the Guadalquivir Bank (Gulf of Cadiz): Interaction between bottom current, mass-wasting and tectonic processes. Mar Geol 378, 5–19. http://dx.doi.org/10.1016/j.margeo.2015.10.004

Gardner, J. V, Prior, D.B., Field, M.E., 1999. Humboldt Slide — a large shear-dominated retrogressive slope failure. Mar Geol 154, 323–338. https://doi.org/10.1016/S0025-3227(98)00121-2

Gascard, J.C., Clarke, R.A., 1983. The Formation of Labrador Sea Water. Part II. Mesoscale and Smaller-Scale Processes. J Phys Oceanogr 13, 1779–1797. https://doi.org/10.1175/1520-0485(1983)013<1779:TFOLSW>2.0.CO;2

Gaudin, M., Mulder, T., Cirac, P., Berne, S., Imbert, P., 2006. Past and present sedimentary activity in the Capbreton Canyon, southern Bay of Biscay. Geo-Marine Lett 26, 331–345. https://doi.org/10.1007/s00367-006-0043-1

Gómez-Ballesteros, M., Druet, M., Muñoz, A., Arrese, B., Rivera, J., Sánchez, F., Cristobo, J., Parra, S., García-Alegre, A., González-Pola, C., Gallastegui, J., Acosta, J., 2014. Geomorphology of the Avilés Canyon System, Cantabrian Sea. Deep Sea Res Part II Top Stud Oceanogr 106, 99–117. http://dx.doi.org/10.1016/j.dsr2.2013.09.031

González-Pola, C., Díaz del Río, G., Ruiz-Villarreal, M., Sánchez, R.F., Mohn, C., 2012. Circulation patterns at Le Danois Bank, an elongated shelf-adjacent seamount in the Bay of Biscay. Deep Sea Res Part I Oceanogr Res Pap 60, 7–21. http://dx.doi.org/10.1016/j.dsr.2011.10.001

Haynes, R., Barton, E.D., 1990. A poleward flow along the Atlantic coast of the Iberian peninsula. J Geophys Res Ocean 95, 11425–11441. https://doi.org/10.1029/JC095iC07p11425

Hernández-Molina, F.J., Llave, E., Ercilla, G., Maestro, A., Medialdea, T., Ferrin, A., Somoza, L., Gràcia, E., Masson, D.G., García, M., Vizcaino, A., León, R., 2008. Recent sedimentary processes in the Prestige site area (Galicia Bank, NW Iberian Margin) evidenced by high-resolution marine geophysical methods. Mar Geol 249, 21–45. https://doi.org/10.1016/j.margeo.2007.09.011

Hernández-Molina, F.J., Llave, E., Preu, B., Ercilla, G., Fontan, A., Bruno, M., Serra, N., Gomiz, J.J., Brackenridge, R.E., Sierro, F.J., Stow, D.A. V, García, M., Juan, C., Sandoval, N., Arnaiz, A., 2014. Contourite processes associated with the Mediterranean Outflow Water after its exit from the Strait of Gibraltar: Global and conceptual implications. Geology 42, 227–230. https://doi.org/10.1130/g35083.1

Hernández-Molina, F.J., Paterlini, M., Somoza, L., Violante, R., Arecco, M.A., de Isasi, M., Rebesco, M., Uenzelmann-Neben, G., Neben, S., Marshall, P., 2010. Giant mounded drifts in the Argentine Continental Margin: Origins, and global implications for the history of thermohaline circulation. Mar Pet Geol 27, 1508–1530. https://doi.org/10.1016/j.marpetgeo.2010.04.003

731 Hernández-Molina, F.J., Wåhlin, A., Bruno, M., Ercilla, G., Llave, E., Serra, N., Rosón, G., Puig, P., Rebesco, M., Van Rooij, D.,
732 Roque, D., González-Pola, C., Sánchez, F., Gómez, M., Preu, B., Schwenk, T., Hanebuth, T.J.J., Sánchez Leal, R.F.,
733 García-Lafuente, J., Brackenridge, R.E., Juan, C., Stow, D.A. V, Sánchez-González, J.M., 2016. Oceanographic
734 processes and morphosedimentary products along the Iberian margins: A new multidisciplinary approach. Mar
735 Geol 378, 127–156. http://dx.doi.org/10.1016/j.margeo.2015.12.008

736 Holland, W.R., 1972. Baroclinic and topographic influences on the transport in western boundary currents. Geophys
737 Fluid Dyn 4, 187–210. https://doi.org/10.1080/03091927208236095

738 Iglesias, J., 2009. Sedimentation on the cantabrian continental margin from late oligocene to quaternary. Unpubl PhD
739 Thesis.

740 Iorga, M.C., Lozier, M.S., 1999a. Signatures of the Mediterranean outflow from a North Atlantic climatology 1. Salinity
741 and density fields. J Geophys Res 104, 25985–26009. https://doi.org/10.1029/1999JC900115

742 Iorga, M.C., Lozier, M.S., 1999b. Signatures of the Mediterranean outflow from a North Atlantic climatology 2.
743 Diagnostic velocity fields. J Geophys Res 104, 26011–26029. https://doi.org/10.1029/1999JC900204

744 Jackson, L., Hughes, C.W., Williams, R.G., 2006. Topographic Control of Basin and Channel Flows: The Role of Bottom
745 Pressure Torques and Friction. J Phys Oceanogr 36, 1786–1805. https://doi.org/10.1175/JPO2936.1

746 Juan, C., Ercilla, G., Javier Hernández-Molina, F., Estrada, F., Alonso, B., Casas, D., García, M., Farran, M., Llave, E.,
747 Palomino, D., Vázquez, J.-T., Medialdea, T., Gorini, C., D'Acremont, E., El Moumni, B., Ammar, A., 2016. Seismic
748 evidence of current-controlled sedimentation in the Alboran Sea during the Pliocene and Quaternary:
749 Palaeoceanographic implications. Mar Geol 378, 292–311. http://dx.doi.org/10.1016/j.margeo.2016.01.006

750 Kaboth, S., Bahr, A., Reichart, G.-J., Jacobs, B., Lourens, L.J., 2016. New insights into upper MOW variability over the last
751 150 kyr from IODP 339 Site U1386 in the Gulf of Cadiz. Mar Geol 377, 136–145.
752 http://dx.doi.org/10.1016/j.margeo.2015.08.014

753 Kaboth, S., de Boer, B., Bahr, A., Zeeden, C., Lourens, L.J., 2017. Mediterranean Outflow Water dynamics during the past
754 ~570 kyr: Regional and global implications. Paleoceanography 32, 634–647.
755 https://doi.org/10.1002/2016PA003063

756 Kvalstad, T.J., Andresen, L., Forsberg, C.F., Berg, K., Bryn, P., Wangen, M., 2005. The Storegga slide: evaluation of
757 triggering sources and slide mechanics. Mar Pet Geol 22, 245–256.
758 https://doi.org/10.1016/j.marpetgeo.2004.10.019

759 Laberg, J.S., Camerlenghi, A., 2008. Chapter 25 The Significance of Contourites for Submarine Slope Stability, in:
760 Rebesco, M., Camerlenghi, A. (Eds.), Developments in Sedimentology. Elsevier, pp. 537–556.
761 http://dx.doi.org/10.1016/S0070-4571(08)10025-5

762 Laberg, J.S., Stoker, M.S., Dahlgren, K.I.T., Haas, H. de, Haflidason, H., Hjelstuen, B.O., Nielsen, T., Shannon, P.M., Vorren,
763 T.O., van Weering, T.C.E., Ceramicola, S., 2005. Cenozoic alongslope processes and sedimentation on the NW
764 European Atlantic margin. Mar Pet Geol 22, 1069–1088. http://dx.doi.org/10.1016/j.marpetgeo.2005.01.008

765 Lamb, K.G., 2014. Internal Wave Breaking and Dissipation Mechanisms on the Continental Slope/Shelf. Annu Rev Fluid
766 Mech 46, 231–254. https://doi.org/10.1146/annurev-fluid-011212-140701

767 Lavín, A., Valdés, L., Sánchez, F., Abaunza, P., Forest, A., Boucher, J., Lazure, P., Jegou, A.M., 2006. The Bay of Biscay: the
768 encountering of the ocean and the shelf, in: Brink, A.R.R.K.H. (Ed.), The Sea. the President and Fellows of
769 Harvard College, pp. 933–999.

770 Lazier, J.R.N., 1973. The renewal of Labrador sea water. Deep Sea Res Oceanogr Abstr 20, 341–353.
771 http://dx.doi.org/10.1016/0011-7471(73)90058-2

772 Lee, H.J., Syvitski, J.P.M., Parker, G., Orange, D., Locat, J., Hutton, E.W.H., Imran, J., 2002. Distinguishing sediment waves
773 from slope failure deposits: field examples, including the 'Humboldt slide', and modelling results. Mar Geol 192,
774 79–104. http://dx.doi.org/10.1016/S0025-3227(02)00550-9

775 Llave, E., Hernandez-Molina, F.J., Somoza, L., Diaz-del Rio, V., Stow, D.A. V, Maestro, A., Alveirinho Dias, J.M., 2001.
776 Seismic stacking pattern of the Faro-Albufeira contourite system (Gulf of Cadiz): a Quaternary record of
777 paleoceanographic and tectonic influences. Mar Geophys Res 22, 487–508.
778 https://doi.org/10.1023/A:1016355801344

779 Llave, E., Schönfeld, J., Hernandez-Molina, F.J., Mulder, T., Somoza, L., Diaz-del Rio, V., Sanchez-Almazo, I., 2006. High-
780 resolution stratigraphy of the Mediterranean outflow contourite system in the Gulf of Cadiz during the late
781 Pleistocene: The impact of Heinrich events. Mar Geol 277, 241–262.
782 https://doi.org/10.1016/j.margeo.2005.11.015

783 Locat, J., Lee, H.J., 2002. Submarine landslides: advances and challenges. Can Geotech J 39, 193–212.
784 https://doi.org/10.1139/t01-089

785 Maldonado, A., Barnolas, A., Bohoyo, F., Escutia, C., Galindo-Zaldívar, J., Hernández-Molina, J., Jabaloy, A., Lobo, F.J.,
786 Nelson, C.H., Rodríguez-Fernández, J., Somoza, L., Vázquez, J.-T., 2005. Miocene to Recent contourite drifts
787 development in the northern Weddell Sea. Glob Planet Change 45, 99–129.
788 http://dx.doi.org/10.1016/j.gloplacha.2004.09.013

789 Masson, D.G., Howe, J.A., Stoker, M.S., 2002. Bottom-current sediment waves, sediment drifts and contourites in the
790 northern Rockall Trough. Mar Geol 192, 215–237. http://dx.doi.org/10.1016/S0025-3227(02)00556-X

791 McCartney, M.S., Mauritzen, C., 2001. On the origin of the warm inflow to the Nordic Seas. Prog Oceanogr 51, 125–214.
792 http://dx.doi.org/10.1016/S0079-6611(01)00084-2

793 Mena, A., Francés, G., Pérez-Arlucea, M., Hanebuth, T.J.J., Bender, V.B., Nombela, M.A., 2018. Evolution of the Galicia
794 Interior Basin over the last 60 ka: sedimentary processes and palaeoceanographic implications. J Quat Sci 33,
795 536–549. https://doi.org/doi:10.1002/jqs.3032

796 Miramontes, E., Cattaneo, A., Jouet, G., Garziglia, S., 2016. Implications of Sediment Dynamics in Mass Transport along
797 the Pianosa Ridge (Northern Tyrrhenian Sea), in: Lamarche, G., Mountjoy, J., Bull, S., Hubble, T., Krastel, S., Lane,
798 E., Micallef, A., Moscardelli, L., Mueller, C., Pecher, I., Woelz, S. (Eds.), Submarine Mass Movements and Their
799 Consequences: 7th International Symposium. Springer International Publishing, Cham, pp. 301–309.
800 https://doi.org/10.1007/978-3-319-20979-1_30 LB - Miramontes2016

801 Mosher, D.C., Thomson, R.E., 2002. The Foreslope Hills: large-scale, fine-grained sediment waves in the Strait of
802 Georgia, British Columbia. Mar Geol 192, 275–295. http://dx.doi.org/10.1016/S0025-3227(02)00559-5

803 Muench, R.D., Wåhlin, A.K., Özgökmen, T.M., Hallberg, R., Padman, L., 2009. Impacts of bottom corrugations on a dense
804 Antarctic outflow: NW Ross Sea. Geophys Res Lett 36. https://doi.org/doi:10.1029/2009GL041347

805 Muñoz, J.A., 2002. The pyrenees. Geol Spain 370–385.

806 Cadenas, P., Fernandez-Viejo, G., 2016. The Asturian Basin within the North Iberian margin (Bay of Biscay): seismic
807 characterisation of its geometry and its Mesozoic and Cenozoic cover. Basin Res 29, 521-541.
808 https://doi.org/doi:10.1111/bre.12187

809 Palomino, D., López-González, N., Vázquez, J.-T., Fernández-Salas, L.-M., Rueda, J.-L., Sánchez-Leal, R., Díaz-del-Río, V.,
810 2016. Multidisciplinary study of mud volcanoes and diapirs and their relationship to seepages and bottom
811 currents in the Gulf of Cádiz continental slope (northeastern sector). Mar Geol 378, 196–212.
812 https://doi.org/10.1016/j.margeo.2015.10.001

813 Pingree, R.D., 1993. Flow of surface waters to the west of the British Isles and in the Bay of Biscay. Deep Sea Res Part II
814 Top Stud Oceanogr 40, 369–388. http://dx.doi.org/10.1016/0967-0645(93)90022-F

815 Pingree, R.D., Le Cann, B., 1992. Three anticyclonic slope water oceanic eDDIES (SWODDIES) in the Southern Bay of
816 Biscay in 1990. Deep Sea Res Part A Oceanogr Res Pap 39, 1147–1175. http://dx.doi.org/10.1016/0198-
817 0149(92)90062-X

818 Pingree, R.D., Le Cann, B., 1990. Structure, strength and seasonality of the slope currents in the Bay of Biscay region. J
819 Mar Biol Assoc United Kingdom 70, 857–885. https://doi.org/10.1017/S0025315400059117

820 Pollard, R.T., Griffttths, M.J., Cunningham, S.A., Read, J.F., Pérez, F.F., Ríos, A.F., 1996. Vivaldi 1991 - A study of the
821 formation, circulation and ventilation of Eastern North Atlantic Central Water. Prog Oceanogr 37, 167–192.
822 http://dx.doi.org/10.1016/S0079-6611(96)00008-0

823 Pomar, L., Morsilli, M., Hallock, P., Bádenas, B., 2012. Internal waves, an under-explored source of turbulence events in
824 the sedimentary record. Earth-Science Rev 111, 56–81. http://dx.doi.org/10.1016/j.earscirev.2011.12.005

825 Prego, R., Boi, P., Cobelo-García, A., 2008. The contribution of total suspended solids to the Bay of Biscay by Cantabrian
826 Rivers (northern coast of the Iberian Peninsula) Bay of Biscay. J Mar Syst 72, 342–349.
827 http://dx.doi.org/10.1016/j.jmarsys.2007.01.011

828 Preu, B., Hernández-Molina, F.J., Violante, R., Piola, A.R., Paterlini, C.M., Schwenk, T., Voigt, I., Krastel, S., Spiess, V., 2013.
829 Morphosedimentary and hydrographic features of the northern Argentine margin: The interplay between
830 erosive, depositional and gravitational processes and its conceptual implications. Deep Sea Res Part I Oceanogr
831 Res Pap 75, 157–174. http://dx.doi.org/10.1016/j.dsr.2012.12.013

832 Preu, B., Schwenk, T., Hernández-Molina, F.J., Violante, R., Paterlini, M., Krastel, S., Tomasini, J., Spieß, V., 2012.
833 Sedimentary growth pattern on the northern Argentine slope: The impact of North Atlantic Deep Water on

southern hemisphere slope architecture. Mar Geol 329–331, 113–125. https://doi.org/10.1016/j.margeo.2012.09.009

Rashid, H., MacKillop, K., Sherwin, J., Piper, D.J.W., Marche, B., Vermooten, M., 2017. Slope instability on a shallow contourite-dominated continental margin, southeastern Grand Banks, eastern Canada. Mar Geol 393, 203–215. https://doi.org/10.1016/j.margeo.2017.01.001

Rebesco, M., Camerlenghi, A., Van Loon, A.J., 2008. Chapter 1 Contourite Research: A Field in Full Development, in: Rebesco, M., Camerlenghi, A. (Eds.), Developments in Sedimentology. Elsevier, pp. 1–10. http://dx.doi.org/10.1016/S0070-4571(08)10001-2

Rebesco, M., Hernández-Molina, F.J., Van Rooij, D., Wåhlin, A., 2014. Contourites and associated sediments controlled by deep-water circulation processes: State-of-the-art and future considerations. Mar Geol 352, 111–154. http://dx.doi.org/10.1016/j.margeo.2014.03.011

Riaza Molina, C., 1996. Inversión estructural en la cuenca mesozoica del off-shore asturiano. Revisión de un modelo exploratorio Geogaceta. Geogaceta 20, 169–171. http://hdl.handle.net/10272/11399

Ribó, M., Puig, P., Muñoz, A., Lo Iacono, C., Masqué, P., Palanques, A., Acosta, J., Guillén, J., Gómez Ballesteros, M., 2016. Morphobathymetric analysis of the large fine-grained sediment waves over the Gulf of Valencia continental slope (NW Mediterranean). Geomorphology 253, 22–37. http://dx.doi.org/10.1016/j.geomorph.2015.09.027

Ríos, A.F., Pérez, F.F., Fraga, F., 1992. Water masses in the upper and middle North Atlantic Ocean east of the Azores. Deep Sea Res Part A Oceanogr Res Pap 39, 645–658. http://dx.doi.org/10.1016/0198-0149(92)90093-9

Roca, E., Muñoz, J.A., Ferrer, O., Ellouz, N., 2011. The role of the Bay of Biscay Mesozoic extensional structure in the configuration of the Pyrenean orogen: Constraints from the MARCONI deep seismic reflection survey. Tectonics 30, TC2001. https://doi.org/10.1029/2010TC002735

Rogerson, M., Rohling, E.J., Bigg, G.R., Ramirez, J., 2012. Paleoceanography of the Atlantic-Mediterranean exchange: Overview and first quantitative assessment of climatic forcing. Rev Geophys 50, RG2003. https://doi.org/10.1029/2011RG000376

Rumín-Caparrós, A., Sanchez-Vidal, A., Calafat, A., Canals, M., Martín, J., Puig, P., Pedrosa-Pàmies, R., 2013. External forcings, oceanographic processes and particle flux dynamics in Cap de Creus submarine canyon, NW Mediterranean Sea. Biogeosciences 10, 3493–3505. https://doi.org/10.5194/bg-10-3493-2013

Rumín-Caparrós, A., Sanchez-Vidal, A., González-Pola, C., Lastras, G., Calafat, A., Canals, M., 2016. Particle fluxes and their drivers in the Avilés submarine canyon and adjacent slope, central Cantabrian margin, Bay of Biscay. Prog Oceanogr 144, 39–61. http://dx.doi.org/10.1016/j.pocean.2016.03.004

Shanmugam, G., 2013. New perspectives on deep-water sandstones: Implications. Pet Explor Dev 40, 316–324. http://dx.doi.org/10.1016/S1876-3804(13)60038-5

Speer, K.G., Gould, J., LaCasce, J., 1999. Year-long float trajectories in the Labrador Sea Water of the eastern North Atlantic Ocean. Deep Sea Res Part II Top Stud Oceanogr 46, 165–179. https://doi.org/10.1016/S0967-0645(98)00103-9

Stoker, M.S., Hoult, R.J., Nielsen, T., Hjelstuen, B.O., Laberg, J.S., Shannon, P.M., Praeg, D., Mathiesen, A., van Weering, T.C.E., McDonnell, A., 2005. Sedimentary and oceanographic responses to early Neogene compression on the NW European margin. Mar Pet Geol 22, 1031–1044. https://doi.org/10.1016/j.marpetgeo.2005.01.009

Stow, D.A.V, Faugères, J.-C., Howe, J.A., Pudsey, C.J., Viana, A.R., 2002. Bottom currents, contourites and deep-sea sediment drifts: current state-of-the-art. Geol Soc London, Mem 22, 7–20. https://doi.org/10.1144/gsl.mem.2002.022.01.02

Stow, D.A.V, Hernández-Molina, F.J., Llave, E., Bruno, M., García, M., Díaz del Rio, V., Somoza, L., Brackenridge, R.E., 2013. The Cadiz Contourite Channel: Sandy contourites, bedforms and dynamic current interaction. Mar Geol 343, 99–114. http://dx.doi.org/10.1016/j.margeo.2013.06.013

Stow, D.A.V, Hunter, S., Wilkinson, D., Hernández-Molina, F.J., 2008. Chapter 9 The Nature of Contourite Deposition, in: Rebesco, M., Camerlenghi, A. (Eds.), Developments in Sedimentology. Elsevier, pp. 143–156. http://dx.doi.org/10.1016/S0070-4571(08)10009-7

Stow, D.A.V, Javier Hernández-Molina, F., Llave, E., Sayago, M., 2009. Bedform-velocity matrix: The estimation of bottom current velocity from bedform observations. Geology 37, 327–330. https://doi.org/10.1130/G25259A.1

Sultan, N., Cochonat, P., Canals, M., Cattaneo, A., Dennielou, B., Haflidason, H., Laberg, J.S., Long, D., Mienert, J., Trincardi, F., Urgeles, R., Vorren, T.O., Wilson, C., 2004. Triggering mechanisms of slope instability processes and sediment failures on continental margins: a geotechnical approach. Mar Geol 213, 291–321.

886 https://doi.org/10.1016/j.margeo.2004.10.011

887 Tugend, J., Manatschal, G., Kusznir, N.J., Masini, E., Mohn, G., Thinon, I., 2014. Formation and deformation of
888 hyperextended rift systems: Insights from rift domain mapping in the Bay of Biscay-Pyrenees. Tectonics 33,
889 1239–1276. https://doi.org/10.1002/2014TC003529

890 Turnewitsch, R., Reyss, J.L., Chapman, D.C., Thomson, J., Lampitt, R.S., 2004. Evidence for a sedimentary fingerprint of
891 an asymmetric flow field surrounding a short seamount. Earth Planet Sci Lett 222, 1023–1036.
892 https://doi.org/10.1016/j.epsl.2004.03.042

893 van Aken, H.M., 2000a. The hydrography of the mid-latitude northeast Atlantic Ocean: I: The deep water masses. Deep
894 Sea Res Part I Oceanogr Res Pap 47, 757–788. http://dx.doi.org/10.1016/S0967-0637(99)00092-8

895 van Aken, H.M., 2000b. The hydrography of the mid-latitude Northeast Atlantic Ocean: II: The intermediate water
896 masses. Deep Sea Res Part I Oceanogr Res Pap 47, 789–824. http://dx.doi.org/10.1016/S0967-0637(99)00112-
897 0

898 Van Rooij, D., Blamart, D., Kozachenko, M., Henriet, J.-P., 2007. Small mounded contourite drifts associated with deep-
899 water coral banks, Porcupine Seabight, NE Atlantic Ocean. Geol Soc London, Spec Publ 276, 225–244.
900 https://doi.org/10.1144/gsl.sp.2007.276.01.11

901 Van Rooij, D., Campbell, C., Rueggeberg, A., Wahlin, A., 2016. The contourite log-book: significance for
902 palaeoceanography, ecosystems and slope instability. Mar Geol 378, 1–4.
903 http://dx.doi.org/10.1016/j.margeo.2016.05.018

904 Van Rooij, D., Iglesias, J., Hernández-Molina, F.J., Ercilla, G., Gomez-Ballesteros, M., Casas, D., Llave, E., De Hauwere, A.,
905 Garcia-Gil, S., Acosta, J., Henriet, J.P., 2010. The Le Danois Contourite Depositional System: Interactions between
906 the Mediterranean Outflow Water and the upper Cantabrian slope (North Iberian margin)(Bay of Biscay). Mar
907 Geol 274, 1–20. http://dx.doi.org/10.1016/j.margeo.2010.03.001

908 Vandorpe, T., Martins, I., Vitorino, J., Hebbeln, D., García, M., Van Rooij, D., 2016. Bottom currents and their influence on
909 the sedimentation pattern in the El Arraiche mud volcano province, southern Gulf of Cadiz. Mar Geol 378, 114–
910 126. https://doi.org/10.1016/j.margeo.2015.11.012

911 Verdicchio, G., Trincardi, F., 2008. Chapter 20 Shallow-Water Contourites, in: Rebesco, M., Camerlenghi, A. (Eds.),
912 Developments in Sedimentology. Elsevier, pp. 409–433. http://dx.doi.org/10.1016/S0070-4571(08)10020-6

913 Vergés, J., Fernàndez, M., Martìnez, A., 2002. The Pyrenean orogen: pre-, syn-, and post-collisional evolution. J Virtual
914 Explor 8, 55–74.

915 Vissers, R.L.M., Meijer, P.T., 2012. Iberian plate kinematics and Alpine collision in the Pyrenees. Earth-Science Rev 114,
916 61–83. https://doi.org/10.1016/j.earscirev.2012.05.001

917 von Lom-Keil, H., Spieß, V., Hopfauf, V., 2002. Fine-grained sediment waves on the western flank of the Zapiola Drift,
918 Argentine Basin: evidence for variations in Late Quaternary bottom flow activity. Mar Geol 192, 239–258.
919 http://dx.doi.org/10.1016/S0025-3227(02)00557-1

920 Weigelt, E., Uenzelmann-Neben, G., 2004. Sediment deposits in the Cape Basin: Indications for shifting ocean currents?
921 Am Assoc Pet Geol Bull 88, 765–780.

922 Wilson, C.K., Long, D., Bulat, J., 2004. The morphology, setting and processes of the Afen Slide. Mar Geol 213, 149–167.
923 https://doi.org/10.1016/j.margeo.2004.10.005

924 Wynn, R.B., Masson, D.G., 2008. Chapter 15 Sediment Waves and Bedforms, in: Rebesco, M., Camerlenghi, A. (Eds.),
925 Developments in Sedimentology. Elsevier, pp. 289–300. http://dx.doi.org/10.1016/S0070-4571(08)10015-2

926 Wynn, R.B., Stow, D.A. V, 2002. Classification and characterisation of deep-water sediment waves. Mar Geol 192, 7–22.
927 http://dx.doi.org/10.1016/S0025-3227(02)00547-9

928 Zhang, W., Hanebuth, T.J.J., Stöber, U., 2016. Short-term sediment dynamics on a meso-scale contourite drift (off NW
929 Iberia): Impacts of multi-scale oceanographic processes deduced from the analysis of mooring data and
930 numerical modelling. Mar Geol 378, 81–100. http://dx.doi.org/10.1016/j.margeo.2015.12.006

931

Fig. 1. Location of the study area: A) Position with respect to the North Iberian continental margin (Ercilla et al., 2008), contour lines every 500 m. Location of the rivers is based on Prego et al. (2008); B) Available geophysical datasets for this study. The present-day oceanographic circulation pattern is modified from González-Pola et al. (2012). The main morphological expressions are shown (contour lines every 100 m). ENACW = Eastern North Atlantic Central Water; AMW = Atlantic Mediterranean Water; LSW = Labrador Sea Water.

Fig. 2. Slope map (in degrees) of the study area, with the location of displayed seismic profiles. The identified contourite deposits (red boxes) and slide scars are indicated.

Fig. 3. (a) 3D colour shaded relief multibeam high-resolution bathymetric map of the study area (ECOMARG project, IEO), with the location of oceanographic cross-sections A-A', B-B' and C-C (World Ocean Database, 2013). (b) Potential temperature versus salinity diagram from the water masses in the study area (World Ocean Database, 2013). CTD stations (red triangles) and their respective locations are indicated in cross-section profiles. (c, d, e, f) Oceanographic cross-sections from the Le Danois Bank towards the Cantabrian continental margin. The water column colour ranges indicate salinity (c, e, f) and temperature (d).

Fig. 4. Morphosedimentary map of the Le Danois Bank region, based on the interpretation of multibeam bathymetry and seismic profiles. Numbers (1-6) and letters (A, B, C) respectively denote plastered drifts and sediment wave fields.

Fig. 5. Interpreted sparker seismic profiles showing the morphological features of elongated mounded and separated drifts and a plastered drift. Onlap and downlap terminations (red arrows) are indicated. The location the of seismic lines is indicated on the slope map (Fig. 2).

Fig. 6. Interpreted sparker (a, b), TOPAS (c, d) and airgun (e) seismic profiles showing the morphological features of plastered drifts and slide scars. Onlap and downlap terminations (red arrows) are indicated. The location of the seismic lines is indicated on the slope map (Fig. 2).

Fig. 7. Interpreted sparker (a, b, d, e) and airgun (c, f) seismic profiles showing the morphological features of slide scars, mass-transport deposits and sediment waves. The location of the seismic lines is indicated on the slope map (Fig. 2).

Fig. 8. Seismic and oceanographic profiles in the Le Danois Bank region. The depth intervals of the water masses and contourite features show the dynamic interaction between water masses and the present-day sedimentary regime. The locations of airgun seismic profiles are indicated in the bathymetric map. The junctions of Line a, b and f; and Line e and g (dotted black lines) are indicated in the seismic profiles. The CTD stations (red triangles) and their respective locations are indicated in the seismic and oceanographic profiles.

Fig. 9. Sketch of the recent sedimentary processes within the Le Danois Bank region. This sketch has been produced based on the morphosedimentary features defined in the morphosedimentary map (Fig. 4).

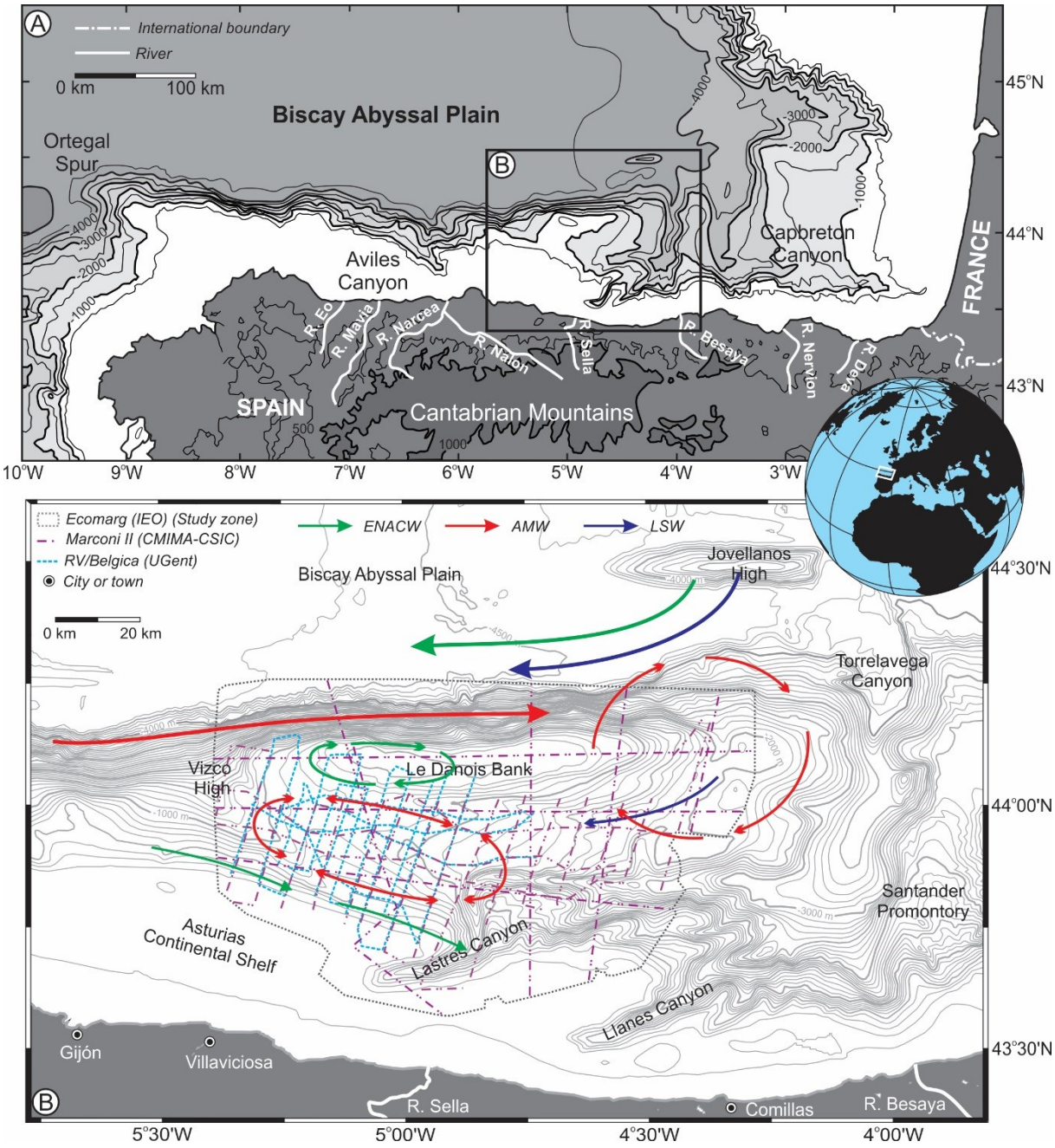
A
International boundary
River
0 km
100 km
Biscay Abyssal Plain
Ortegal Spur
B
Aviles Canyon
Capbreton Canyon
FRANCE
SPAIN
Cantabrian Mountains
R. Eo
R. Navia
R. Narcea
R. Nalon
R. Sella
R. Besaya
R. Nervion
R. Deva
45°N
44°N
43°N
10°W
9°W
8°W
7°W
6°W
5°W
4°W
3°W
Ecomarg (IEO) (Study zone)
Marconi II (CMIMA-CSIC)
RV/Belgica (UGent)
City or town
0 km
20 km
ENACW
AMW
LSW
Biscay Abyssal Plain
Jovellanos High
Torrelavega Canyon
Vizco High
Le Danois Bank
Asturias Continental Shelf
Lastres Canyon
Llanes Canyon
Santander Promontory
Gijón
Villaviciosa
R. Sella
Comillas
R. Besaya
44°30'N
44°00'N
43°30'N
5°30'W
5°00'W
4°30'W
4°00'W

967

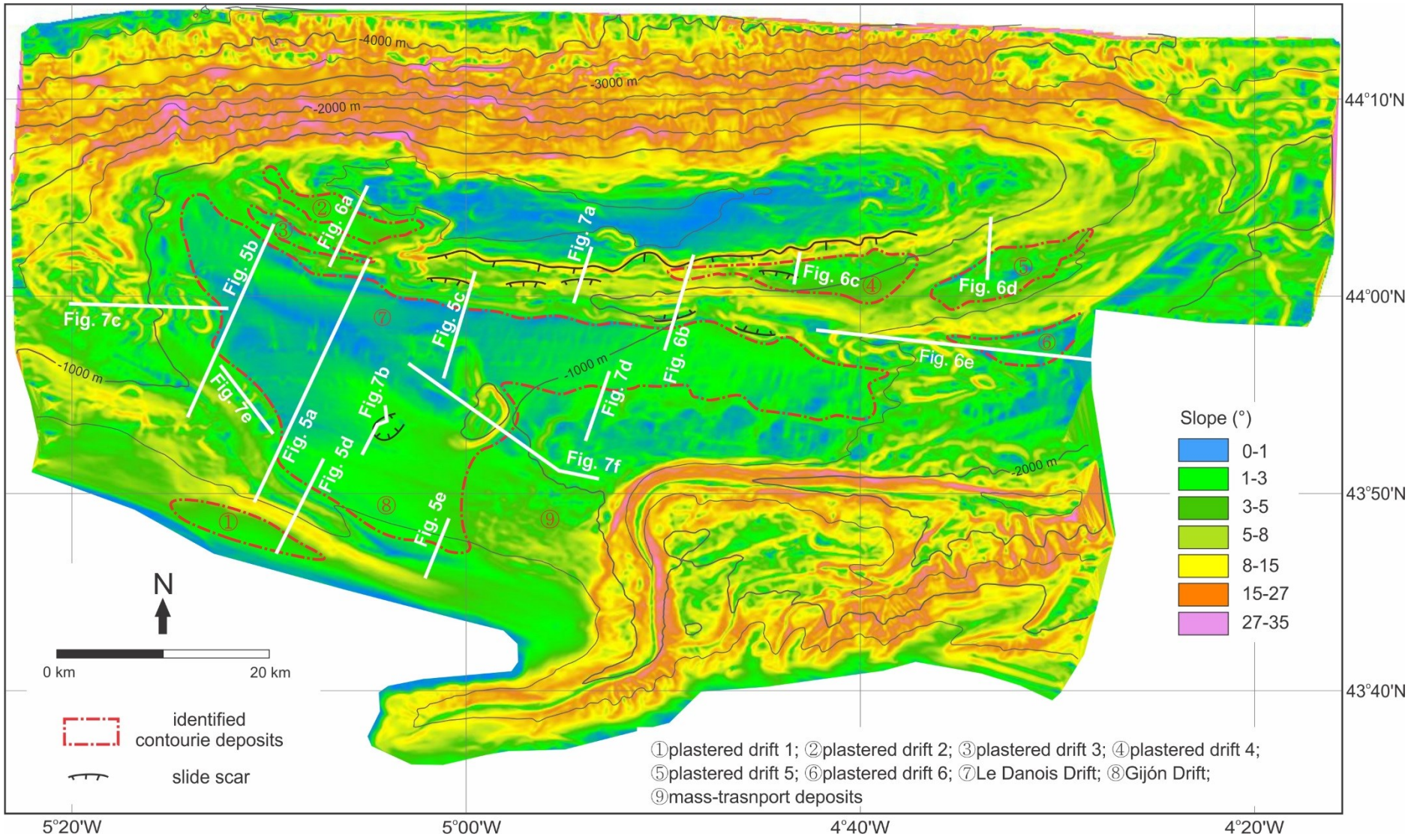
-4000 m
-3000 m
-2000 m
-1000 m
-1000 m
-2000 m
Fig. 5b
Fig. 6a
Fig. 7a
Fig. 6c
Fig. 6d
Fig. 7c
Fig. 5c
Fig. 6b
Fig. 6e
Fig. 7e
Fig. 5a
Fig. 7b
Fig. 7d
Fig. 5d
Fig. 7f
Fig. 5e
①
②
③
④
⑤
⑥
⑦
⑧
⑨
N
0 km
20 km
identified contourie deposits
slide scar
Slope (°)
0-1
1-3
3-5
5-8
8-15
15-27
27-35
①plastered drift 1; ②plastered drift 2; ③plastered drift 3; ④plastered drift 4;
⑤plastered drift 5; ⑥plastered drift 6; ⑦Le Danois Drift; ⑧Gijón Drift;
⑨mass-trasnport deposits
44°10'N
44°00'N
43°50'N
43°40'N
5°20'W
5°00'W
4°40'W
4°20'W

968

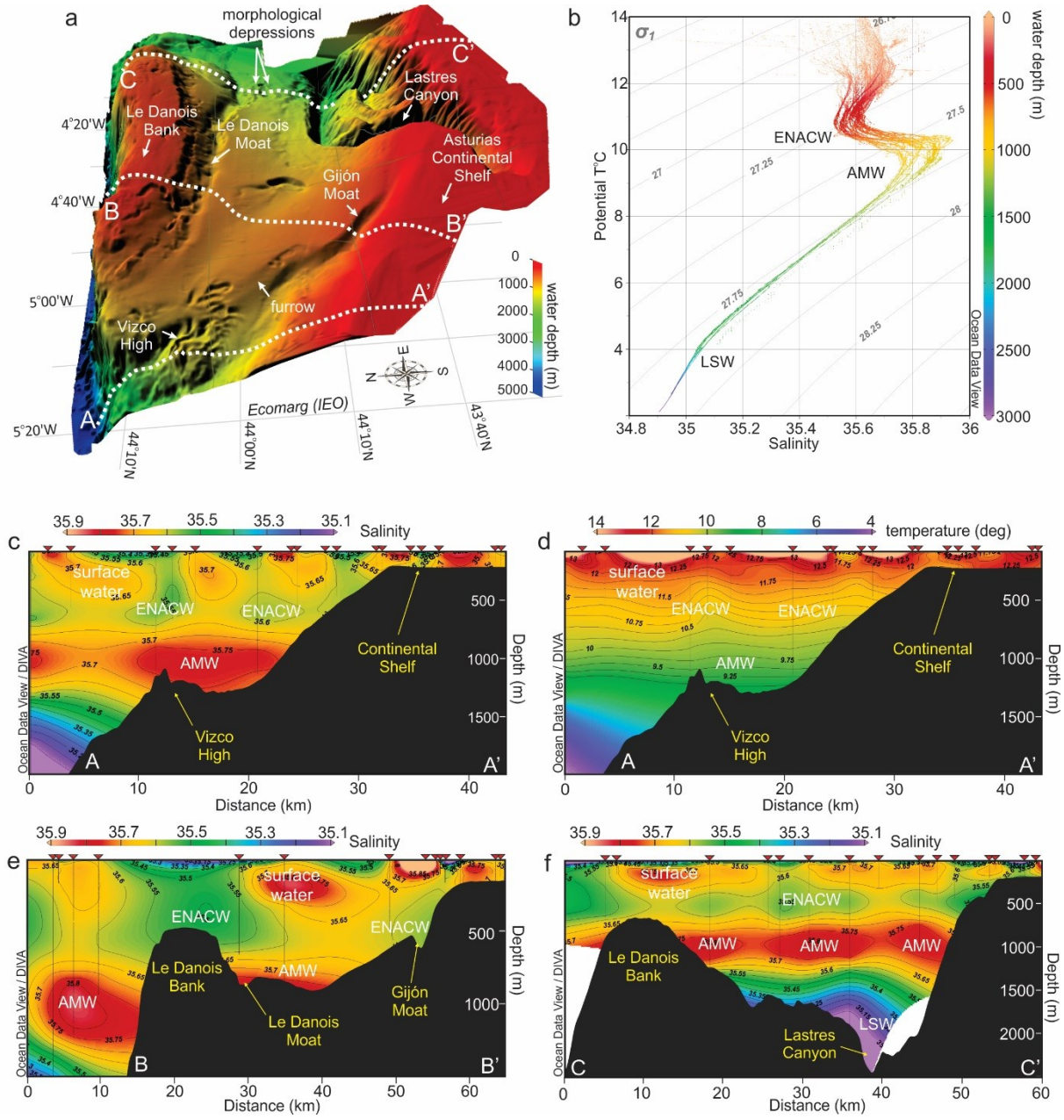
a
morphological depressions
C
C'
Lastres Canyon
Le Danois Bank
Le Danois Moat
Asturias Continental Shelf
Gijón Moat
B
B'
A
A'
furrow
Vizco High
4°20'W
4°40'W
5°00'W
5°20'W
44°10'N
44°00'N
44°10'N
43°40'N
Ecomarg (IEO)
water depth (m)
b
σ1
ENACW
AMW
LSW
Potential T°C
Salinity
Ocean Data View
water depth (m)
c
Salinity
surface water
ENACW
AMW
Continental Shelf
Vizco High
Ocean Data View / DIVA
Depth (m)
Distance (km)
d
temperature (deg)
e
Le Danois Bank
Le Danois Moat
Gijón Moat
f
Lastres Canyon
LSW

969

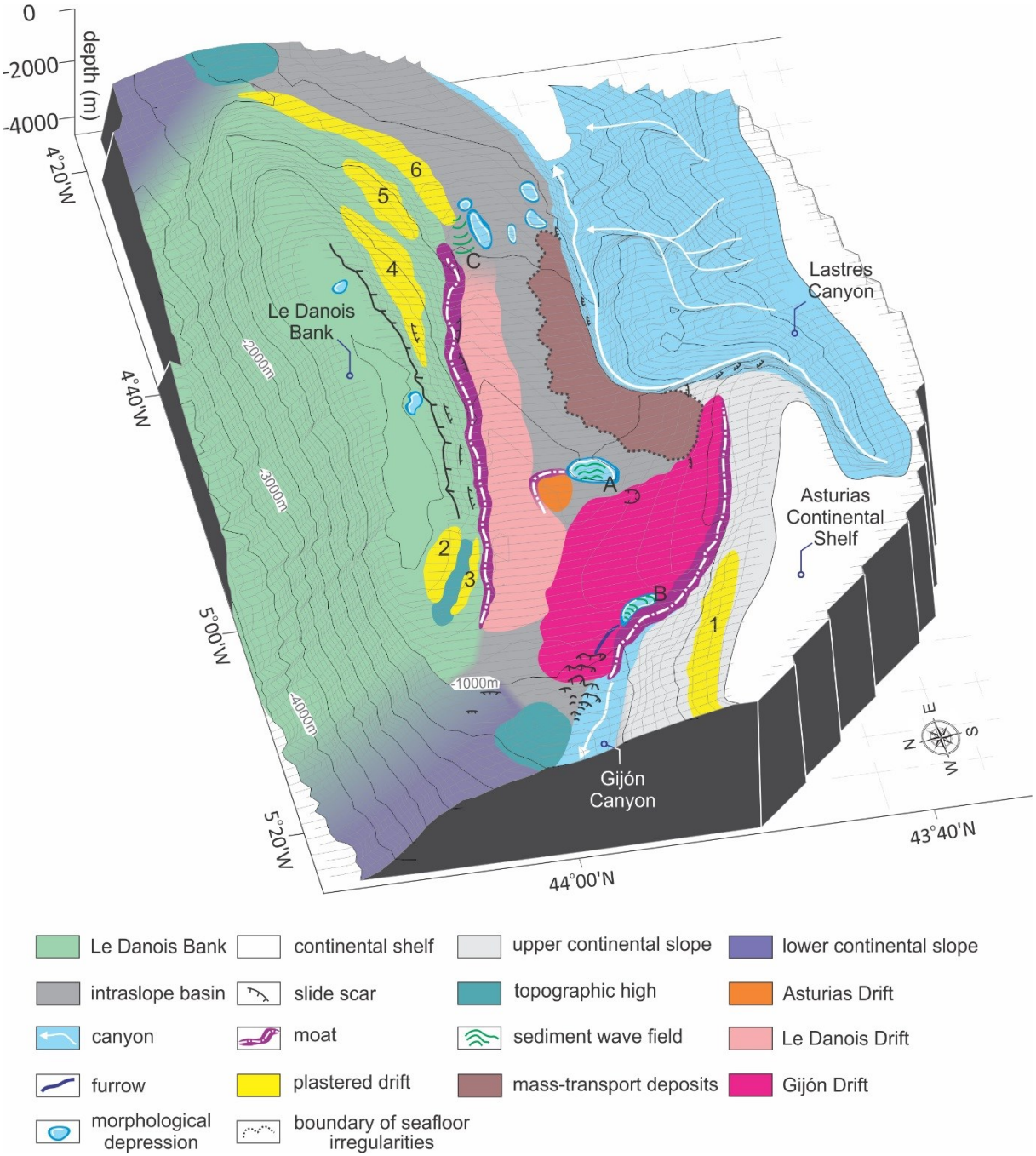
0
-2000
-4000
depth (m)
4°20'W
4°40'W
5°00'W
5°20'W
44°00'N
43°40'N
Le Danois Bank
Lastres Canyon
Asturias Continental Shelf
Gijón Canyon
2000m
3000m
4000m
1000m
A
B
C
1
2
3
4
5
6
N
E
S
W
Le Danois Bank
continental shelf
upper continental slope
lower continental slope
intraslope basin
slide scar
topographic high
Asturias Drift
canyon
moat
sediment wave field
Le Danois Drift
furrow
plastered drift
mass-transport deposits
Gijón Drift
morphological depression
boundary of seafloor irregularities

970

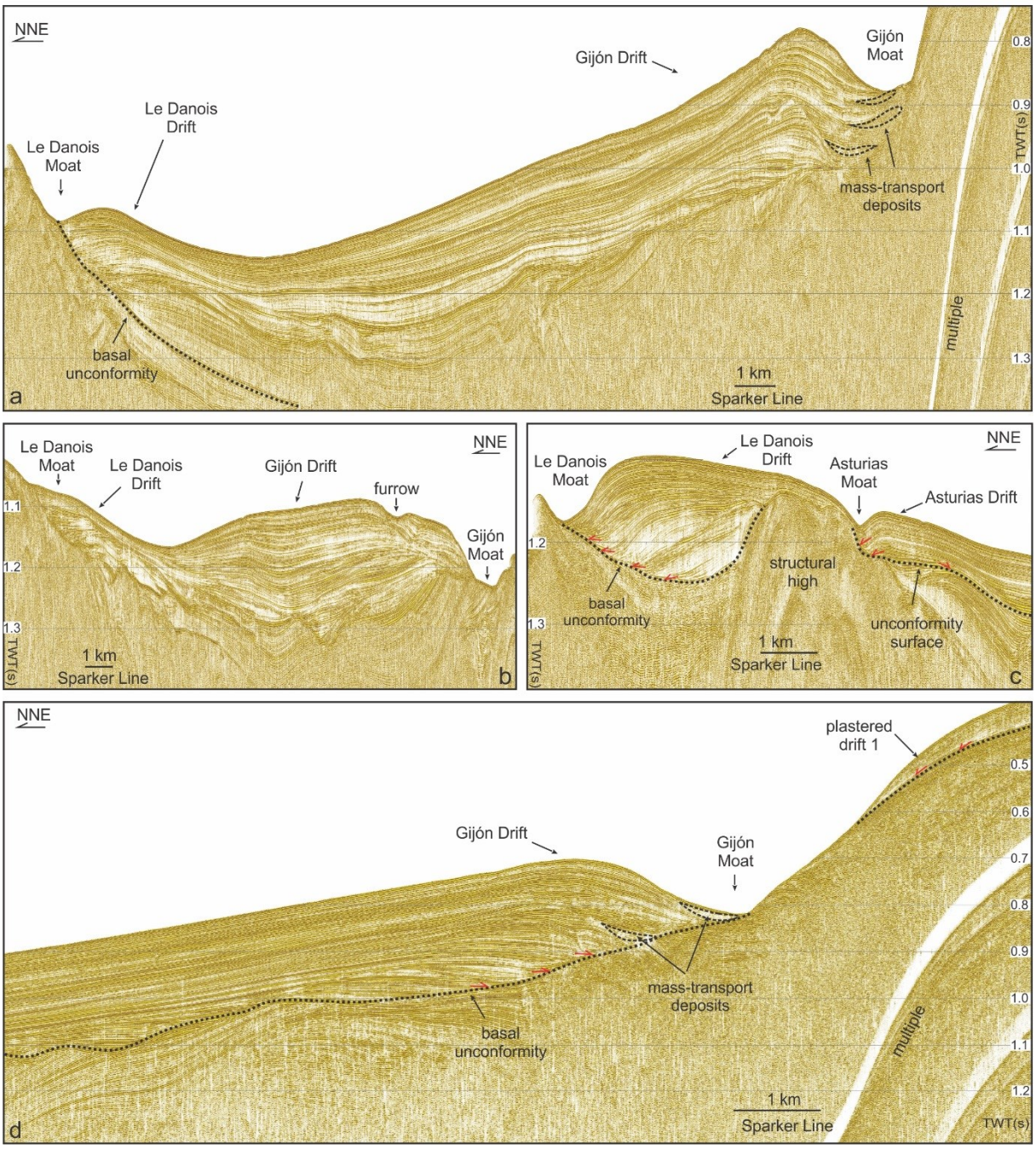
NNE
Gijón Drift
Gijón Moat
Le Danois Drift
Le Danois Moat
mass-transport deposits
basal unconformity
multiple
1 km
Sparker Line
TWT(s)
a
Le Danois Moat
Le Danois Drift
Gijón Drift
furrow
Gijón Moat
b
Le Danois Moat
Le Danois Drift
Asturias Moat
Asturias Drift
structural high
basal unconformity
unconformity surface
c
plastered drift 1
Gijón Drift
Gijón Moat
mass-transport deposits
basal unconformity
d

971

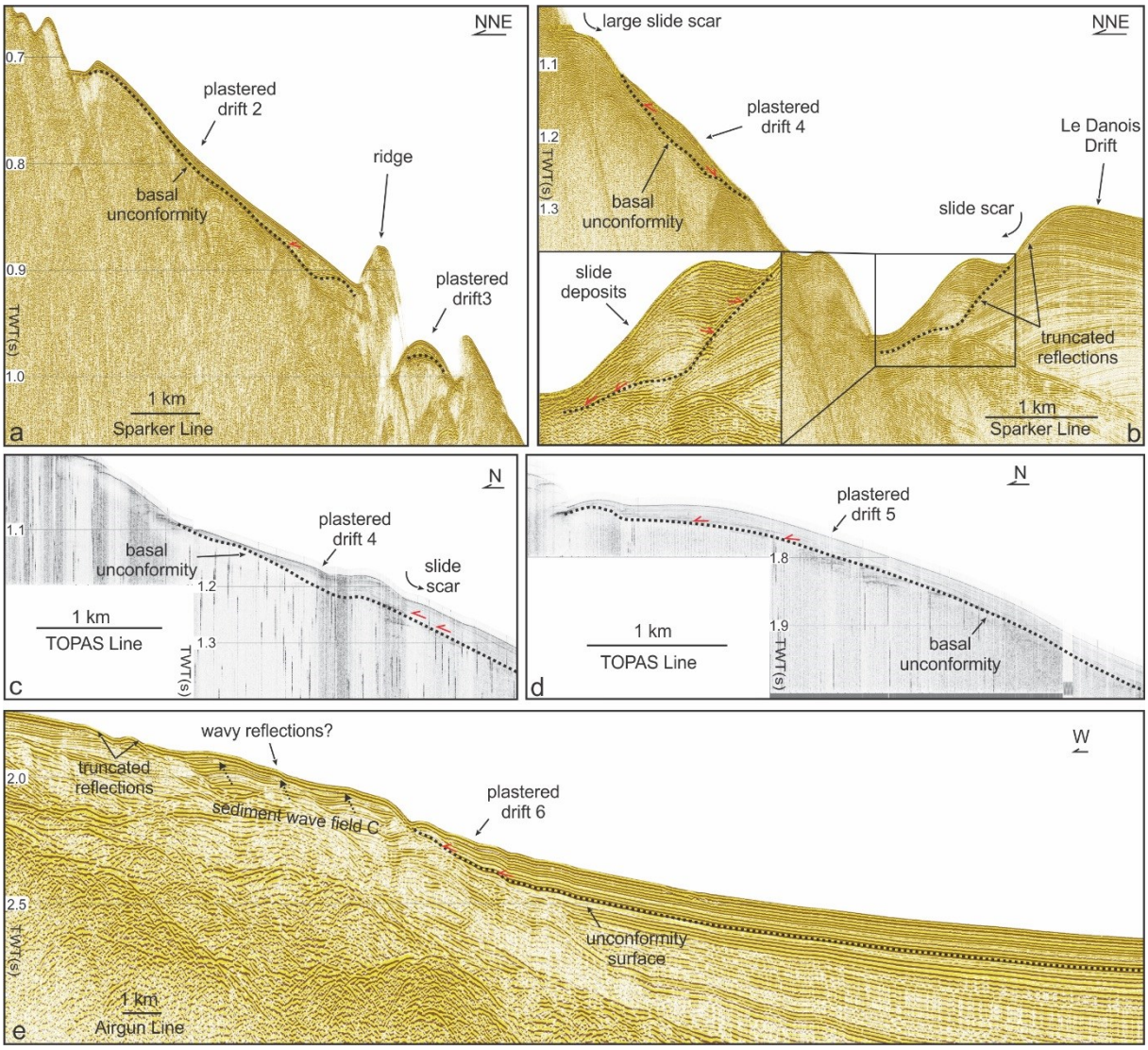
NNE
0.7
plastered
drift 2
0.8
basal
unconformity
ridge
0.9
plastered
drift3
TWT(s)
1.0
1 km
Sparker Line
a
large slide scar
NNE
1.1
plastered
drift 4
1.2
TWT(s)
1.3
basal
unconformity
Le Danois
Drift
slide scar
slide
deposits
truncated
reflections
1 km
Sparker Line
b
N
1.1
basal
unconformity
plastered
drift 4
slide
scar
1.2
1 km
TOPAS Line
1.3
TWT(s)
c
N
plastered
drift 5
1.8
1 km
TOPAS Line
1.9
TWT(s)
basal
unconformity
d
wavy reflections?
W
truncated
reflections
2.0
sediment wave field C
plastered
drift 6
2.5
TWT(s)
unconformity
surface
1 km
Airgun Line
e

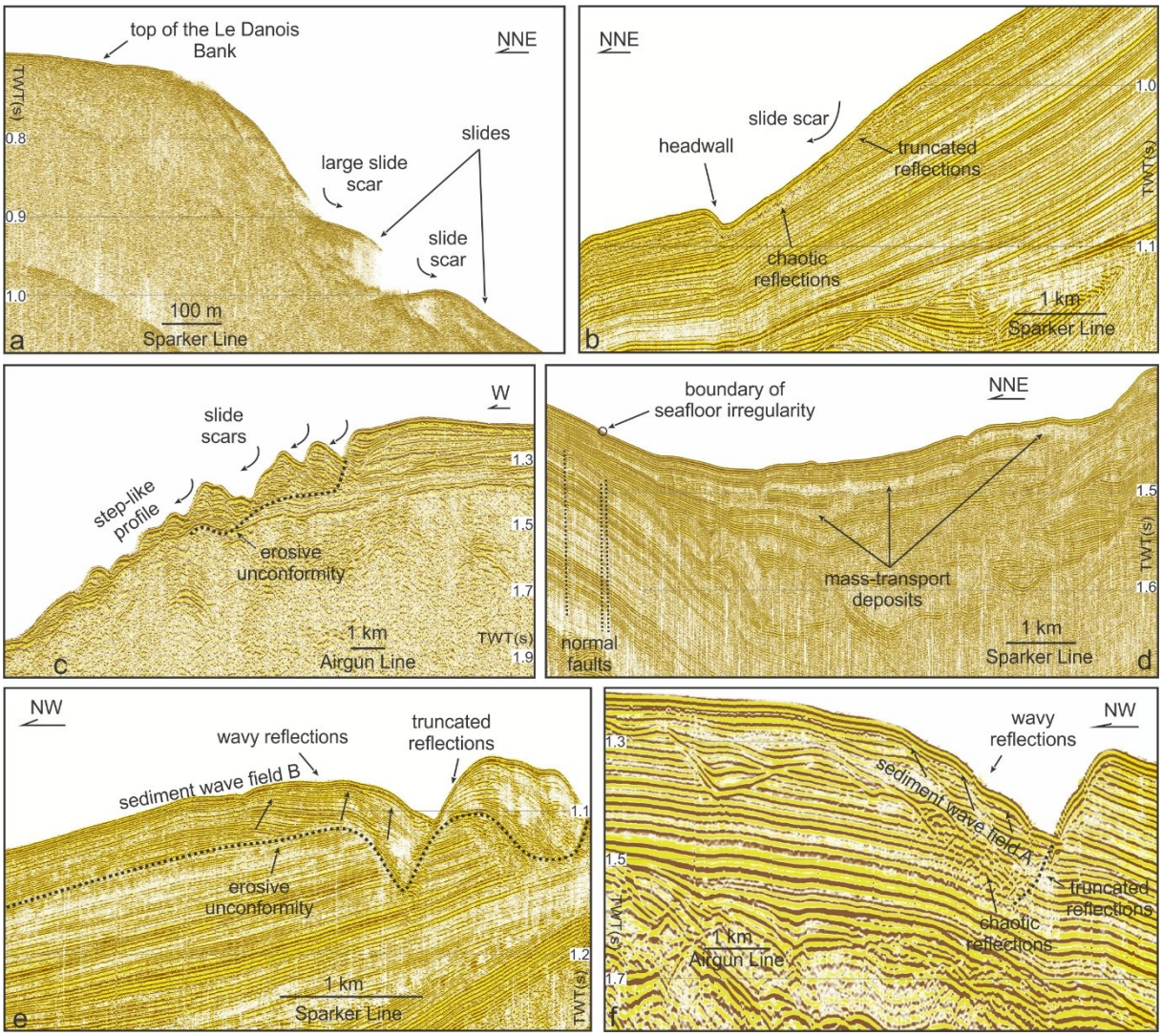
top of the Le Danois Bank
NNE
TWT(s)
0.8
0.9
1.0
slides
large slide scar
slide scar
100 m
Sparker Line
a
NNE
1.0
slide scar
headwall
truncated reflections
TWT(s)
chaotic reflections
1.1
1 km
Sparker Line
b
W
slide scars
1.3
step-like profile
1.5
erosive unconformity
1.7
1 km
Airgun Line
TWT(s)
1.9
c
boundary of seafloor irregularity
NNE
1.5
TWT(s)
mass-transport deposits
1.6
1 km
Sparker Line
normal faults
d
NW
wavy reflections
truncated reflections
sediment wave field B
1.1
erosive unconformity
1 km
Sparker Line
1.2
TWT(s)
e
NW
wavy reflections
1.3
sediment wave field A
1.5
truncated reflections
TWT(s)
chaotic reflections
1 km
Airgun Line
1.7
f

973

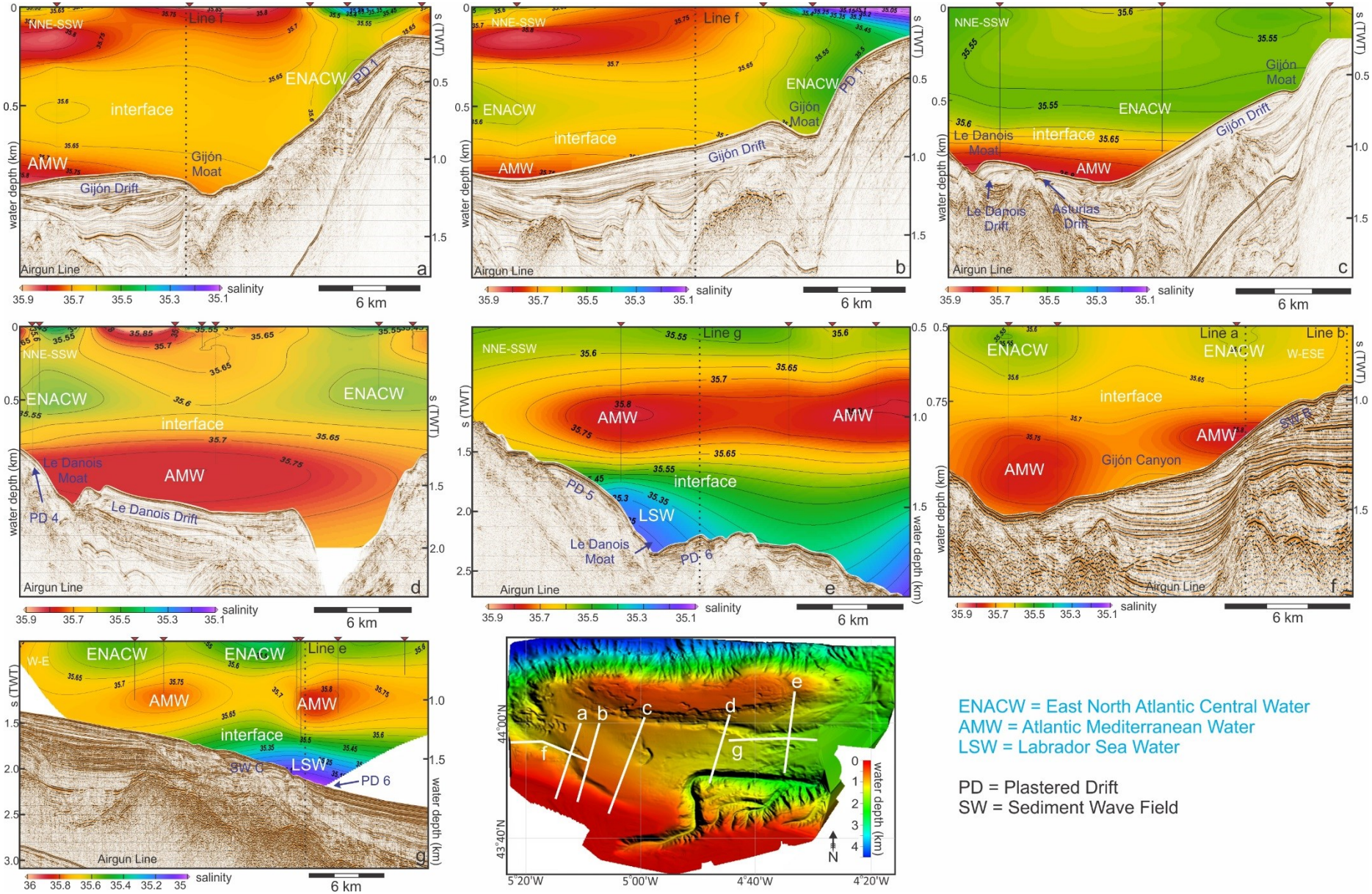

ENACW = East North Atlantic Central Water
AMW = Atlantic Mediterranean Water
LSW = Labrador Sea Water

PD = Plastered Drift
SW = Sediment Wave Field

974

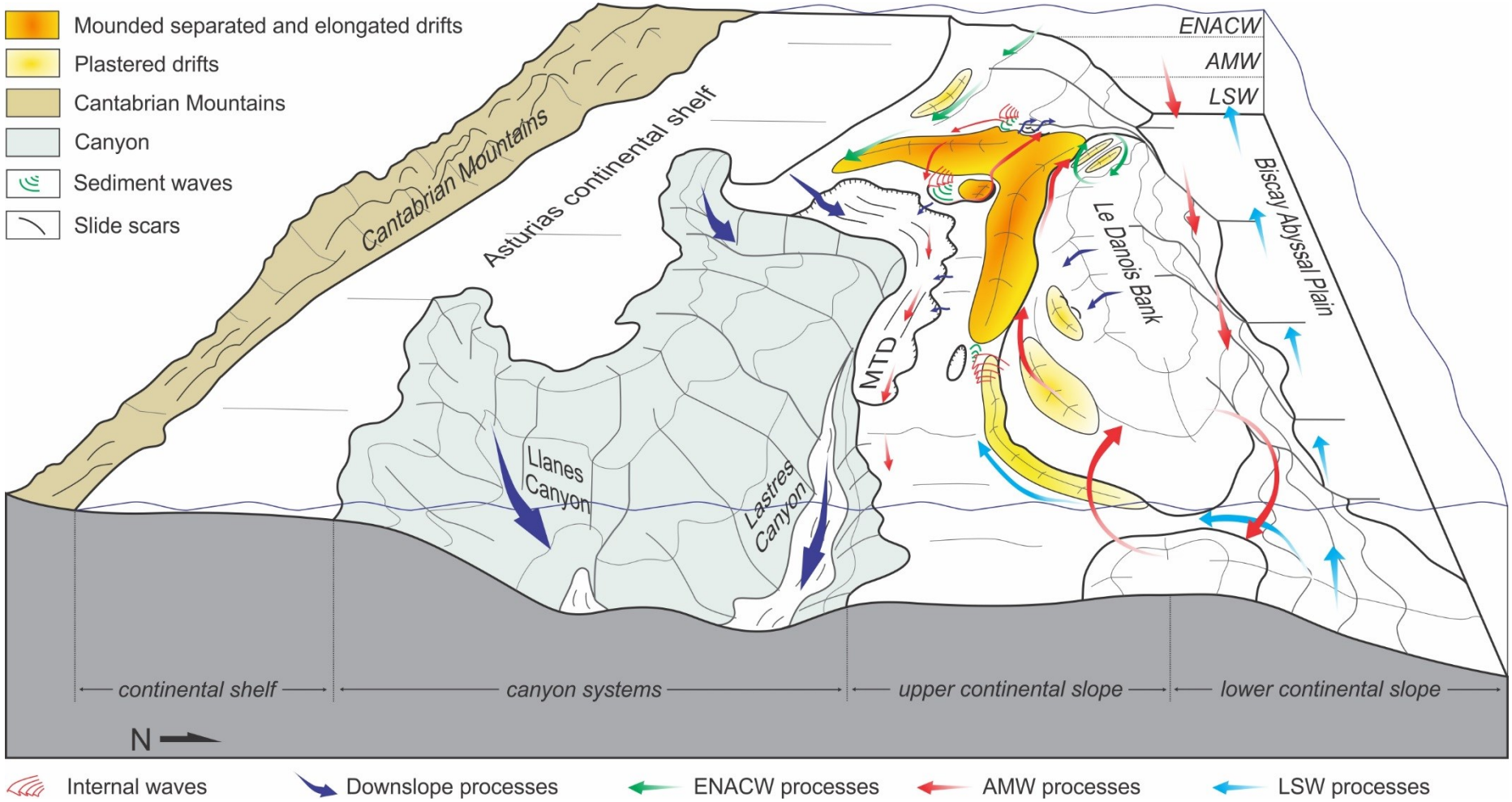
Mounded separated and elongated drifts
Plastered drifts
Cantabrian Mountains
Canyon
Sediment waves
Slide scars
Cantabrian Mountains
Asturias continental shelf
ENACW
AMW
LSW
Biscay Abyssal Plain
Le Danois Bank
MTD
Llanes Canyon
Lastres Canyon
continental shelf
canyon systems
upper continental slope
lower continental slope
N
Internal waves
Downslope processes
ENACW processes
AMW processes
LSW processes

975